CHAPTER ONE
1. INTRODUCTION

1.1 General View

Ultrasound or ultrasonography is a medical imaging technique that uses high frequency sound waves and their echoes; known as a 'pulse echo technique', which is similar to the echolocation used by bats and dolphins, as well as SONAR used by submarines [1].

Ultrasound imaging is an efficient, noninvasive, method for medical diagnosis [2].because of its efficacy and low cost, it is often the preferred imaging modality. Millions of people have been spared painful exploratory surgery by noninvasive imaging. Their lives have been saved by ultrasound diagnosis and timely intervention, their hearts have been evaluated and repaired, their children have been found in need of medical help by ultrasound imaging, and their surgeries have been guided and checked by ultrasound [3].

Ultrasound has been used to image the human body for over half a century. Dr. Karl Theo Dussik, an Austrian neurologist, was the first to apply ultrasound as a medical diagnostic tool to image the brain. Today, ultrasound (US) is one of the most widely used imaging technologies in medicine. It is portable, free of radiation risk, and relatively inexpensive when compared with other imaging modalities, such as magnetic resonance and computed tomography. The images can be acquired in "real time," thus providing instantaneous visual guidance for many interventional procedures including

those for regional anesthesia and pain management [4]. The next figure (Figure 1.1) shows an example of ultrasound images.

Figure 1.1: Obstetrical ultrasound images demonstrating both 2D (right) and 3D (left) reconstructions [5]

Ultrasound compared to other medical imaging techniques:

Compared to other medical imaging techniques (like MRI, CT and X-ray) the advantages of ultrasound are [4]:

- It images muscle and soft tissue very well and is particularly useful for delineating the interfaces between solid and fluid-filled spaces.
- It renders "live" images, where the operator can dynamically select the most useful section for diagnosing and documenting changes, often enabling rapid diagnoses.
- It has no known long-term side effects and rarely causes any discomfort to the patient.
- Equipment is widely available, flexible, Small, easily carried scanners are available; examinations can be performed at the bedside.
- Relatively inexpensive compared to CT and MRI.

Ultrasound machines have three distinct subsystems: the transducer and its cable assembly, the front-end electronics, and the back-end computer with its user interface and display. One of the most critical components of the front-end electronics is the beam-former [6].

Beam-forming techniques play one of the most important roles in ultrasound imaging, beam-former has two functions: the transmit beam-forming responsible for dynamic focusing, the receive beam-forming responsible for alignment. Beam-former can be either analog or digital. Traditional ultrasound systems use analog beam-former technology (The time delays required for beam-forming can be accomplished by analog delay lines); these analog delay lines impose significant limitations on the beam-former performances, e.g. limited focusing accuracy, and susceptibility to changes in value over time and temperature [7].

Digital beam-forming, as applied to the medical ultrasound, is defined as phase alignment and summation [8] of signals that are generated from a common source, by received at different times by a multi-elements ultrasound transducer [9].

With the growing availability of high-end integrated analog front-end circuits, distinction between different digital ultrasound imaging systems is determined almost exclusively by their software component [10].

Recently, portable and lightweight ultrasound scanners have been developed, which greatly expand the range of situations and sites for which medical Ultrasound can be used. The evolution of ultrasound scanners is directly influenced by developments in analog and digital electronics. The number of

functions and image quality increases, and the implementation price for any given function decreases with time. One powerful approach for increasing the flexibility and compactness of an ultrasound scanner is to move processing functions from analog to digital electronics.

The project focuses on the part of US system which generates brightness modulation (B-Mode) images out of digitalized radio frequency (RF) data obtained by the ultrasound probe.

1.2 The Problem Statement

The inability of universities and educational centers to provide ultrasound equipments for students training because of their expensive price; hence the relevance of students to them is limited, also students understanding to all signal processing methodologies for digital beam-forming and how to generate brightness modulation (B-mode) images out of digitalized radio frequency (RF) are bounded.

According to the problem which is related to ultrasound price it was necessary to develop low cost educational software medical ultrasound system for students training.

1.3 Thesis Objectives

The general objectives are:

1- Testing signal processing methodologies for ultrasound digital beam-forming.

2- Assist students in understanding the necessary processing steps for transform digital radio frequency data into brightness modulation images.

The specific objective of the project is to develop a compact educational tool-box for digital ultrasound beam-forming that has almost all of its processing steps done on the personal computer (PC) side using MATLAB program.

The new tool will provide the users with a framework for all processing pipeline.

1.4 Methodology

The thesis methodology is about how to develop an educational software tool-box for ultrasound beam-forming using MATLAB as a programming language and to build a Graphical user interface.

The project focuses on the part of ultrasound system which generates B-Mode images out of digitalized RF data obtained by the ultrasound probe. Brightness modulation image is reconstructed using physical array elements for linear and phase array probe (using Linear Array reconstruction and linear phase array reconstruction techniques).

B-Mode images are used to make reflections of ultrasound waves within the body visible for humans. They show a two-dimensional map of the scanned body region based on ultrasound data.

1.5 Thesis Layout

The project thesis consists of six chapters which are:

Chapter one introduces general view for research, problem statement, objectives and methodology.

Chapter two describes theoretical background.

Chapter three represents thesis literature reviews.

Chapter four illustrates research methodology.

Chapter five shows results and their discussions.

Chapter six includes conclusion and future recommendations.

CHAPTOR TWO
2. THEORATICAL BACKGROUND

This section aims to demonstrate US wave's characteristics and their behavior in various media which is essential to understanding the use of diagnostic ultrasound in clinical medicine. The description of medical US equipment and its components, modes, US beam shape and US transducers are shown, as well as the role of each component in US image formation. There is also description for techniques of signal processing which are used to provide better US image quality. Finally some US image artifacts have illustrated

2.1 Ultrasound waves characteristic

US waves are defined as sound with a frequency higher than 20 kHz. It has widespread use in diagnostic imaging where it is associated with low risks and costs. The frequency range for diagnostic applications is 1-30 MHz [11, 12].

2.1.1 Waves Motion

Acoustic waves are mechanical waves i.e. acoustic energy is transferred between two points in the medium. Mechanical waves are of two fundamental types [13]:

- Longitudinal: the oscillating particles of the medium are displaced parallel to the direction of motion (direction of energy transfer).

- Transverse: the oscillating particles of the medium are displaced in a direction perpendicular to the motion of the wave.

Transverse waves:

A simple and familiar example is a wave on the surface of a pond caused by a stone being thrown into the water. The surface of the water at each point in the pond, as shown by a floating object (Figure 2.1), simply goes up and down like a weight on the end of a spring, giving rise to the oscillating nature of the wave. Energy is transported across the pond from the stone to the shore [12].

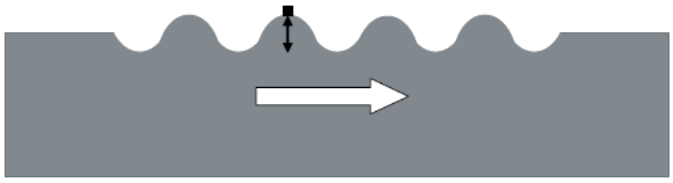

Figure 2.1: The disturbance travel across the ponds [12]

Sound waves:

The sound waves used to form medical images are longitudinal waves, which propagate (travel) through a physical medium (usually tissue or liquid). Here, the particles of the medium oscillate backwards and forwards along the direction of propagation of the wave (Figure 2.2).

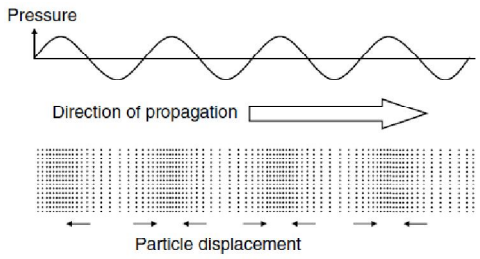

Figure 2.2: In a longitudinal wave particle motion is aligned with the direction of travel, result in bands of high and low pressure [12]

2.1.2 Ultrasound Wave length and Frequency

The frequency of an ultrasound wave consists of the number of cycles or pressure changes that occur in 1 sec. The units are cycles per second or hertz. Frequency is determined by the sound source only and not by the medium in which the sound is traveling. Propagation speed is the speed at which sound can travel through a medium and is typically considered 1540 m/sec for soft tissue. The speed is determined solely by the medium characteristics, especially those of density and stiffness [14].

The wavelength and frequency of US are inversely related, i.e., ultrasound of high frequency has a short wavelength and vice versa. US waves have frequencies that exceed the upper limit for audible human hearing, i.e., greater than 20 kHz. Medical ultrasound devices use sound waves in the range of 1 - 20 MHz [4, 15].

High-frequency ultrasound waves (short wavelength) generate images of high axial resolution. However, high-frequency waves are more attenuated than lower frequency waves for a given distance; thus, they are suitable for imaging mainly superficial structures. Conversely, low-frequency waves offer images of lower resolution but can penetrate to deeper structures due to a lower degree of attenuation (Figure 2.3 and Figure 2.4) [4, 16].

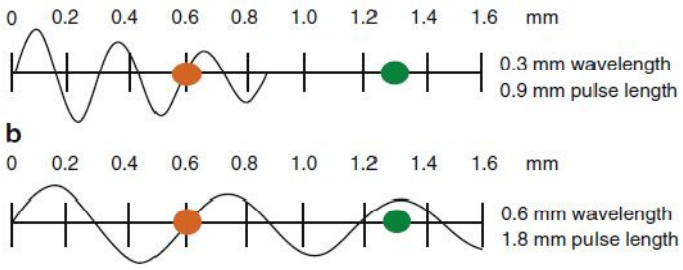

Figure 2.3: Attenuation of US waves and its relation to wave frequency [4]

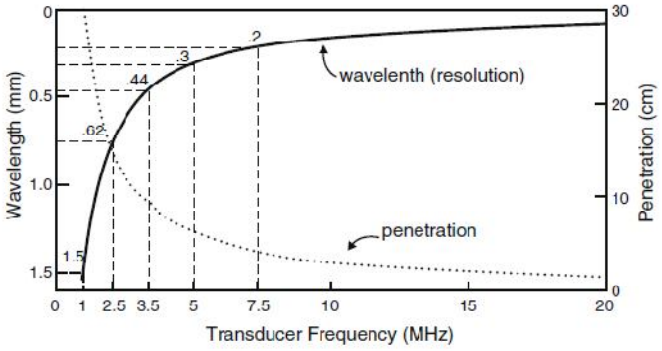

Figure 2.4: A comparison of the resolution and penetration of different US transducer frequencies [16].

Ultrasound waves are generated in pulses that commonly consist of two or three sound cycles of the same frequency (Figure 2.5). The pulse repetition frequency (PRF) is the number of pulses emitted by the transducer per unit of time [4]. The PRF for medical imaging devices ranges from 1 to 10 kHz [4].

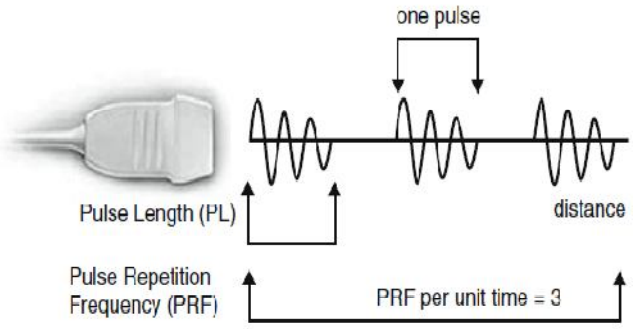

Figure 2.5: Schematic representation of US pulse generation [4].

2.2 Ultrasound and Material Properties

When an US wave travels through a homogenous material it has a constant velocity. The velocity is higher in high-density materials, such as solids, than in low-density materials, such as air [11].

The product of the velocity of sound c and the density ρ gives the acoustic impedance Z of the material, as shown in Eq.2-1 [11].

$$Z = c\rho \qquad \text{(Eq.2-1)}$$

Table 2.1 gives values of Z for some common types of human tissue, air and water. Table 2.1 shows that values for Z in most human soft tissues are very similar [12].

Table2.1: Values of acoustic impedance [12]

Material	z (kg m^{-2} s^{-1})
Liver	1.66×10^6
Kidney	1.61×10^6
Blood	1.67×10^6
Fat	1.33×10^6
Water	1.48×10^6
Air	430
Bone	6.47×10^6

The fact that different materials have different acoustic impedances is the basis of US imaging [12].

2.3 Ultrasound – Tissue Interaction

As US waves travel through tissues, they are partly transmitted to deeper structures, partly reflected back to the transducer as echoes, partly scattered, and partly transformed to heat. For imaging purposes, we are mostly interested in the echoes reflected back to the transducer. The amount of echo returned

after hitting a tissue interface is determined by a tissue property which is (acoustic impedance) [4].

2.3.1 Reflection

In most diagnostic applications of ultrasound, use is made of ultrasound waves reflected from interfaces between different tissues in the patient [17].

When a sound wave travelling through one medium meets an interface with a second medium of different acoustic impedance, some of the wave is transmitted into the second medium and some is reflected back into the first medium. The amplitudes of the transmitted and reflected waves depend on the change in acoustic impedance [12].

Reflection occurs at tissue boundaries and tissue interfaces. With a large impedance mismatch at an interface, much of the energy of an ultrasound wave is reflected, and only a small amount is transmitted across the interface [17].

(Figure 2.6) shows a sound wave travelling through a medium with acoustic impedance Z_1, incident on an interface with a second medium with acoustic impedance Z_2 [12].

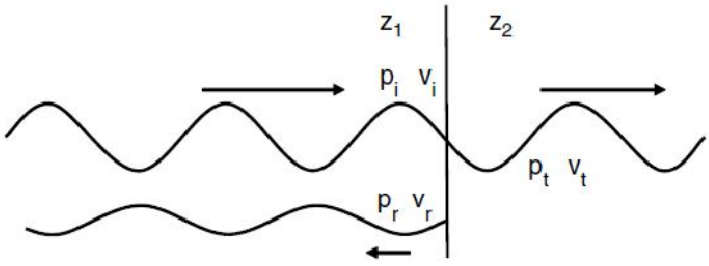

Figure 2.6: Sound wave travelling through two medium [12].

However, the motion of the particles of the medium, and hence their pressure and velocity, must be continuous across the interface to avoid disruption of the medium. To achieve this, the total wave pressure and velocity at the interface in medium 1 must equal those in medium 2 near to the interface [12]. From this condition it can be shown that:

$$\frac{p_r}{p_i} = \frac{z_2 - z_1}{z_2 + z_2} \qquad \text{(Eq.2-2)}$$

Where, P_i and P_r are the pressure amplitudes of the incident and reflected waves respectively near the interface.

This ratio of reflected to incident pressure is commonly referred to as the amplitude reflection coefficient R_A [12]. Table 2.2 shows values of amplitude reflection coefficient for some interfaces that might be encountered in the body. For most soft tissue to soft tissue interfaces, the amplitude reflection coefficient is less than 0.01 (1%) [12].

Table 2.2: Amplitude-reflection coefficient of interfaces [12]

Interface	R_A
Liver–kidney	0.006
Kidney–spleen	0.003
Blood–kidney	0.009
Liver–fat	0.11
Liver–bone	0.59
Liver–air	0.9995

The intensity reflection coefficient describes the ratio of the intensities of the reflected (I_r) and incident waves (I_i). As intensity is proportional to pressure squared, the intensity reflection coefficient (R_i) is given by [12]:

$$\frac{I_r}{I_i} = R_i = R_A{}^2 = \left(\frac{Z_2 - Z_1}{Z_2 + Z_{1^2}}\right)^2 \qquad \text{(Eq.2-3)}$$

The intensity transmission coefficient $T_i = I_t / I_i$ and from above it can be shown that $T_i = 1 - R_i$ [12].

When an incident ultrasound pulse encounters a large, smooth interface of two body tissues with different acoustic impedances, the sound energy is reflected back to the transducer. This type of reflection is called specular reflection as shown in (Figure 2.7) [18].

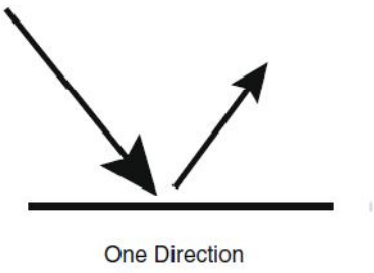

Figure 2.7: Specular reflection [18]

For a flat, smooth interface, the angle of reflection $\theta_r = \theta_i$ the angle of incidence. This is referred to as the law of reflection [18].

2.3.2 Scattering

Reflection, as just described occurs at large interfaces such as those between organs, where there is a change in acoustic impedance [19, 20].

Reflections from small targets do not follow the laws of reflection for large interfaces. When an ultrasound wave is incident on such a target, the wave is scattered over a large range of angles (Figure 2.8) [19].

If a large number of small tissue boundaries occur, the scattering can radiate in all directions. The signal that reaches the transducer is a much weaker signal than the transmitted signal and is typically 100-1000 (40 - 60 dB) less than the transmitted signal. A filter can ignore small signals from red blood cells below a threshold value [17].

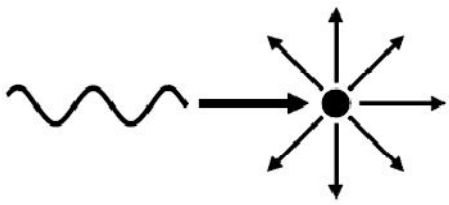

Figure 2.8: Small targets scatter the wave over a large angle [20]

The description of reflection given above assumed a perfectly flat, smooth interface. Some surfaces within the body may be slightly rough on the scale of a wavelength and reflect ultrasound waves over a range of angles, an effect similar to scattering from small targets as shown in (Figure 2.9). This type of reflection is known as diffuse reflection [19].

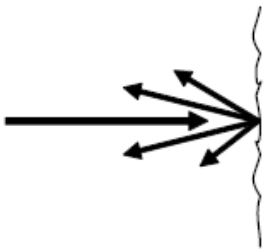

Figure 2.9: Rough surface reflects the wave over a range of angles [20]

2.3.3 Refraction

Refraction refers to a change in the direction of sound transmission after hitting an interface of two tissues with different speeds of sound transmission. In this instance, because the sound frequency is constant, the wavelength has to change to accommodate the difference in the speed of sound transmission in the two tissues [4].

This results in a redirection of the sound pulse as it passes through the interface. Refraction is one of the important causes of incorrect localization of a structure on an ultrasound image [21].

If the velocity of ultrasound is higher in the second medium, then the beam enters this medium at a more oblique (less steep) angle and vice versa. The relationship between incident and refraction angles is described by Snell's law [17]:

$$\frac{\sin \theta_i}{\sin \theta_r} = \frac{c_i}{c_r} \qquad \text{(Eq.2-4)}$$

Where $\theta_i and \theta_r$ represent incidence angle and refractive angle, $c_i and c_r$ represent velocity in incidence medium and velocity in refractive medium [17].

2.3.4 Absorption:

Absorption is the process by which ultrasound energy is converted into heat in the medium [12]. As discussed earlier, ultrasound is propagated by displacement of molecules of a medium into regions of compression and

rarefaction, this displacement requires energy that is provided to the medium by the source of ultrasound. As the molecules attain maximum displacement from an equilibrium position, their motion stops, and their energy is transformed from kinetic energy associated with motion to potential energy associated with position in the compression zone. Actually, the conversion of kinetic to potential energy (and vice versa) is always accompanied by some dissipation of energy. Therefore, the energy of the ultrasound beam is gradually reduced as it passes through the medium [22].

2.3.5 Attenuation

As US pulses travel through tissue, their intensity is reduced or attenuated, this attenuation is the result of reflection and scattering and also of friction-like losses [23].

Reflection and refraction occur at surfaces that are large compared with the wavelength of the ultrasound. For objects that are small in comparison with the wavelength, energy is scattered in many directions, and the eventual fate of the ultrasound is to be absorbed as particle vibration and the production of heat (Figure 2.10) [12].

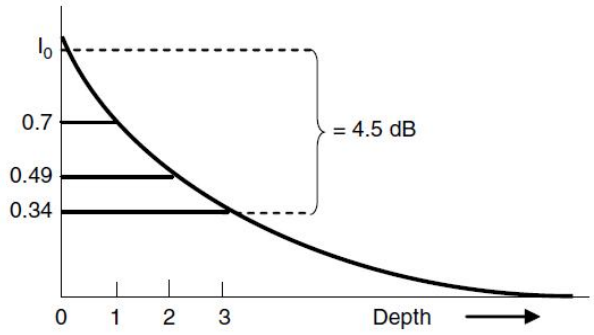

Figure 2.10: US attenuation with distance [12].

Dependence on frequency:

The amount of attenuation varies with the frequency of ultrasound. A high-frequency beam will be attenuated more than a lower frequency. Unfortunately, because higher frequencies enable finer detail to be resolved, there must therefore be a compromise between resolution and penetration for different imaging applications [14].

The attenuation coefficient of most tissues, when expressed in dB cm^{-1}, increases approximately linearly with frequency. Hence, for most tissues, it is possible to measure ultrasound attenuation in dB cm^{-1} MHz^{-1} [24].

2.4 Ultrasound Equipments

Diagnostic imaging is a multi step process as shown in (Figure 2.11) by which information concerning patient anatomy and physiology is gathered and displayed with the modern technology [1].

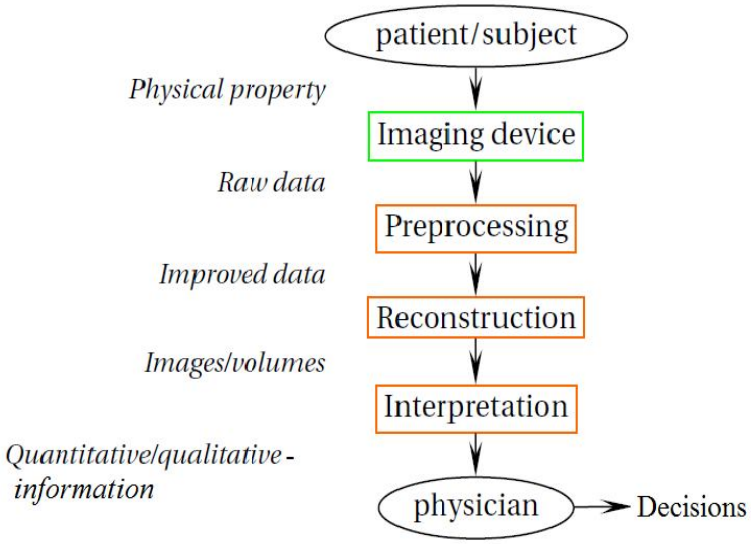

Figure 2.11: Medical imaging pipeline example [1]

In the 1960's the principals of sonar (developed extensively during the Second World War) were applied to diagnostic imaging. The process involves placing a small device called a transducer, against the skin of the patient near the region of interest, for example, the kidneys. This transducer produces a stream of inaudible, high frequency sound waves which penetrate into the body and bounce off the organs inside. The transducer detects sound waves as they bounce off or echo back from the internal structures and contours of the organs. These waves are received by the ultrasound machine and turned into live pictures with the use of computers and reconstruction software [1].

Ultrasound equipment basically consists of a transducer, scanner, computer and monitor [25].

The transducer, also called an ultrasound probe, emits pulses of sound waves between 3.5 to 7.0 megahertz. The central processing unit (CPU) is the brain of the ultrasound machine. The CPU is basically a computer that contains the microprocessor, memory, amplifiers and power supplies for the microprocessor and transducer probe. The CPU sends electrical currents to the transducer probe to emit sound waves, and also receives the electrical pulses from the probes that were created from the returning echoes [25, 26].

The scanner is often part of the transducer and operates to collect the reflection of the sound waves that return after bouncing off the internal systems. The ultrasound equipment may also be connected to a printer, video recorder or data storage device that can make a copy of the scan for later reference [25, 26]. In (Figure 2.12), the external parts of an ultrasound imaging system are shown.

The image **display** is mounted on a chassis with wheels for portability [27, 28]. On the right side, several **transducer arrays** are stored, awaiting use, and they are attached to the system through several **transducer connector bays** in the front. Below the display are a **keyboard** and a number of **knobs** and **switches** for controlling the system. **Peripheral devices**, such as recording media and extra connectors, can be seen. The all-important **on/off switch**, which is sometimes difficult to find, is also identified.

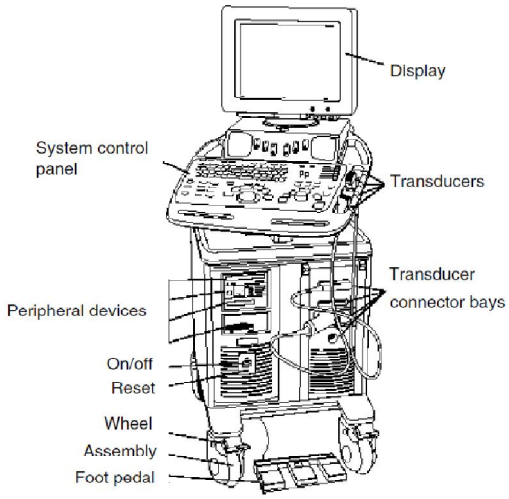

Figure 2.12: External parts of an ultrasound imaging system (courtesy of Philips Medical Systems) [27].

2.4.1 Major Controls [27, 28, 29]

Because there are many controls for a typical ultrasound imaging system and their organization and names vary considerably from manufacturer to manufacturer. The following description is a short list of the major controls according to functions. A close-up of the system control panel of the same imaging system from (Figure 2.12) is illustrated in (Figure 2.13), are the following:

Probe or transducer selection: Typically two to four transducers can be plugged into connectors in the imaging system, so this switch allows the user to activate one of the arrays at a time.

Mode selection: This provides the means for selecting a mode of operation.

Depth of scan control: This adjusts the field of view (scan depth in centimeters).

Focus or transmit focal length selection: This allows the location of the transmit focal length to be moved into a region of interest.

Time gain compensation (TGC) controls: These controls offset the loss in signal caused by tissue absorption.

Transmit level control: This adjusts drive amplitude from transmitters.

Display controls: Primarily, these controls allow optimization of the presentation of information on the display and include a logarithmic compression control, selection of preprocessing and post processing curves, and color maps.

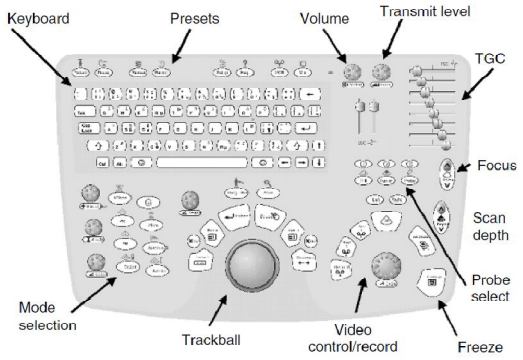

Figure 2.13: Keyboard of an ultrasound imaging system (courtesy of Philips Medical Systems) [27]

2.4.2 Ultrasound Block Diagram

The hidden interior of a digital imaging system is represented functionally by

a generic simplified block diagram (shown by Figure 2.14); a description of this block diagram follows [30]:

User interface: Most of the blocks are hidden from the user, who mainly sees the keyboard and display. This is the part of the system by which the user can configure the system to work in a desired mode of operation.

Controller (computers): A typical system will have one or more microprocessors or a PC that directs the operation of the entire system. It orchestrates the necessary setup of transmit and receive beam-formers as well as the signal processing, display, and output functions.

Front end: This grouping within the scanner is the gateway of signals going in and out of the selected transducer. Under microprocessor transmit control, excitation pulses are sent to the transducer from the transmitter circuitry. Pulse-echo signals from the body are received by array elements and go through individual user-adjustable TGC amplifiers to offset the weakening of echoes by body attenuation and diffraction with distance. These signals then pass on to receive beam-former.

Scanner (beam-forming and signal processing): These parts of the signal chain provide the important function of organizing the many signals of the elements into coherent timelines of echoes for creating each line in the image. Transmit beam-former sends pulses to the elements. Echo signals pass through an analog-to digital (A/D) converter for digital beam-forming.

Back end: This grouping of functions is associated with image formation, display, and image metrics. The input to this group of functions is a set of

pulse-echo envelope lines formed from each beam-formed radiofrequency (RF) data line. Image formation is achieved by organizing the lines and putting them through a digital scan converter that transforms them into a raster scan format for display on a video or PC monitor.

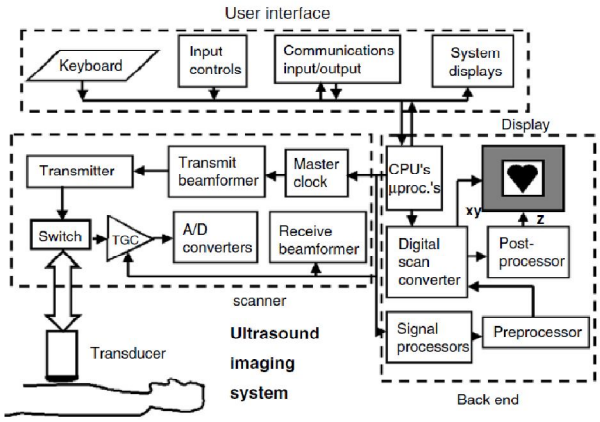

Figure 2.14: Block diagram of digital ultrasound imaging system [30]

2.4.3 Ultrasound major modes

There are different modes of ultrasound imaging. The most common modes are [25]:

- A-mode (Amplitude Mode).
- M-mode - to assess moving body parts (e.g. cardiac movements) from the echoed sound.
- B-mode – the basic two-dimensional intensity mode.
- Doppler-mode - pseudo coloring based on the detected cell motion using Doppler analysis.

A-Mode

In the A-mode presentation of ultrasound images, echoes returning from the

body are displayed as signals on an oscilloscope. The oscilloscope presents a graph of voltage (representing echo amplitude hence the term “A-mode”) on the *y*-axis, as a function of time on the *x*-axis. A-mode reveals the location of echo-producing structures only in the direction of the ultrasound beam. It has been used in the past to localize echo-producing interfaces such as midline structures in the brain (echoencephalography) and structures to be imaged in B-mode [15].

M-Mode

In M-mode (motion mode) ultrasound, pulses are emitted in quick succession each time; either an A-mode or B-mode image is taken. This approach is used for the analysis of moving organs. Over time, this is analogous to recording a video in ultrasound. As the organ boundaries that produce reflections move relative to the probe, this can be used to determine the velocity of specific organ structures [25].

B-Mode

B-mode (Brightness mode) involves transmitting small pulses of ultrasound echo from a transducer into the body. In this case the A-mode information is shown as pixel intensity on a monitor. As the ultrasound waves penetrate body tissues of different acoustic impedances along the path of transmission, some are reflected back to the transducer (echo signals) and some continue to penetrate deeper. Thus, an ultrasound transducer works both as a speaker (generating sound waves) and a microphone (receiving sound waves). B-mode can be used to study both stationary and moving structures but high frame rate is needed to study motion [25, 30].

Doppler-Mode

Doppler ultrasound is a special ultrasound technique that evaluates blood flow through a blood vessel. Doppler ultrasound measures the direction and speed of blood cells as they move through vessels [25].

Doppler Effect: change in frequency of sound due to the relative motion of the source and receiver. There are three types of Doppler ultrasound [25]:

- Color Doppler uses a computer to convert Doppler measurements into an array of colors to visualize the speed and direction of blood flow - through a blood vessel.

- Power Doppler is more sensitive than color Doppler and capable of providing greater detail of blood flow,. Power Doppler, however, does not help the radiologist determine the direction of blood flow.

- Spectral Doppler: Instead of displaying Doppler measurements visually, Spectral Doppler displays blood flow measurements graphically, in terms of the distance traveled per unit of time.

2.4.4 Clinical Applications

Diagnostic ultrasound has found wide application for different parts of the human body. The major categories of ultrasound imaging are [3]:

Breast: Imaging of female (usually) breasts, **Cardiac:** Imaging of the heart, **Gynecologic:** Imaging of the female reproductive organs, **Radiology:** Imaging of the internal organs of the abdomen, **Obstetrics:** Imaging of fetuses

in vivo, **Pediatrics:** Imaging of children, **Vascular:** Imaging of the arteries and veins of the vascular system.

2.4.5 Ultrasound Beam Shape

An ideal ultrasound beam would be one that is very narrow throughout its whole length. This would allow fine detail to be resolved at all imaged depths [12]. The beam from a disk-shaped transducer consists of two parts: the region near the source where the interference of wavelets is most apparent is termed the **Fresnel (or near) zone**. For a disk-shaped transducer of radius *r*, the length *D* of the Fresnel zone is [15]:

$$D_{fresenel} = \frac{r^2}{\lambda} \qquad \text{(Eq.2-5)}$$

Where, λ is the ultrasound wavelength. Within the Fresnel zone, most of the ultrasound energy is confined to a beam width no greater than the transducer diameter as shown in (figure 2.15). Beyond the Fresnel zone, some of the energy escapes along the periphery of the beam to produce a gradual divergence of the ultrasound beam that is described by [15]:

$$\sin(\theta) = 0.6 * \frac{\lambda}{r} \qquad \text{(Eq.2-6)}$$

Where, θ is the Fraunhofer divergence angle in degree, the region beyond the Fresnel zone is termed the Fraunhofer (or far) zone.

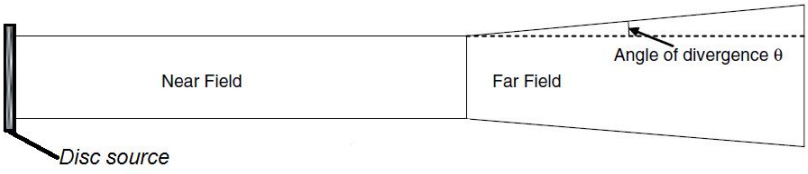

Figure 2.15: US beam shape from a plane disc source [12]

Beam focusing and steering:

A travelling plane wave will tend to spread from the edges as it travels using a process of diffraction. The further the wave has traveled, the greater the reduction in wave amplitude, and the greater the reduction in amplitude of any reflections from the wave. In order to create a high amplitude wave-front (to improve the echo strength) the energy from the wave can be focused. Focusing the wave controls the travel path of the acoustic energy so that its signal strength is maximized within a desired region [٣١].

Focusing can be achieved by:

- Using crystal element shaped by concave curvature, Here the degree of focusing depend on the extent of curvature (radius of curvature), it is internal focusing because it is affected in the crystal itself, as shown in (Figure 2.16) [25].
- Using acoustic lenses made from material which propagates ultrasound at different velocities. It is external focusing as in (Figure 2.17) [25].
- Electronic Focusing: It is employed in multi-crystal transducer. It provides variable/dynamic focusing [25].

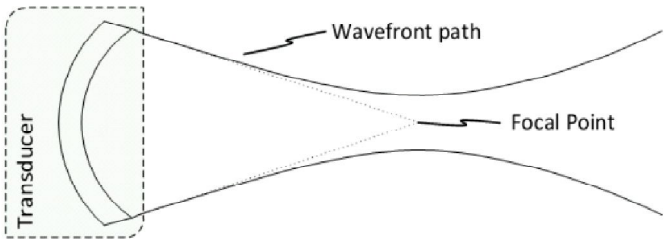

Figure 2.16: US beam with a concave crystal [٣١]

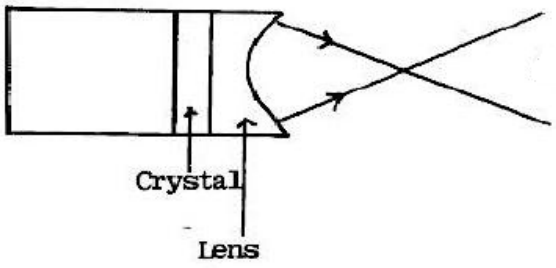

Figure 2.17: US beam focused with acoustic lens [25]

The transducer shown in (Figure 2.16) is geometrically focused, which means that the focal point is determined by the curvature of the transducer. The same effect could also be achieved by using an acoustic lens. In either case, the focal point cannot be easily changed, and for this reason geometrically-focused transducers have limited use in a clinical setting. In order to be able to control the focus, a new type of transducer needs to be considered, and a new way of exciting it. An array transducer divides the transducer surface into sub regions, each of which can be controlled separately through separate electrical connections. The subdivided regions of an array are referred to as elements.

When each element in an array is excited at different times, the diffraction of the individual wave fronts generated from each element can be planned in order to create a focused pulse (Electronic Focusing). This process is called **transmit focusing** [32].

Receive focusing (beam-forming):

After a sound pulse is transmitted, the transducer begins to listen for reflections. When the reflections arrive back at the transducer they are converted into electrical signals.

In this case, the fundamental frequency of the transducer acts as a carrier signal, with its amplitude indicating the reflection size. The echo signal is extracted by taking the envelope of the received signal [33].

In a geometrically focused transducer, signals from the focal region will arrive at the same time at the transducer surface, and thus create a large electrical signal. In an array, however, the signals will all arrive at different times at each element. These situations are shown in (Figure 2.18a and b) [32].

The differences in signal arrival time at each element need to be compensated for by delaying the electrical signals after they are received. If the same transmit delays are applied to the received signals, then waves originating from the focal region will constructively interfere, increasing their amplitude. Signals from outside of this region will not be aligned, and will tend to destructively interfere, reducing their impact on the final output (Figure 2.18c) [36]. The process of delaying the received signals in order to create focus is called **beam-forming** [32].

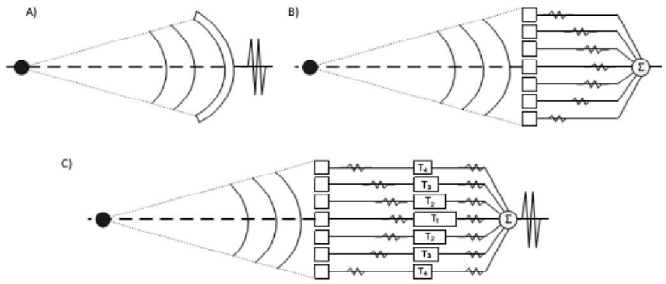

Figure 2.18: Receive focus beam-forming a) geometric transducer b) array without delays c) Array with delays [32]

In addition, since beam-forming delays are applied as the signals are received; it is possible to change the delays during reception. Since there is a different

fixed delay for signals from different depths, we can sweep our receive focal point as the signals are collected to keep an entire line of received data in focus during a single transmit [34]. This process of changing the receive delays while the signal is being received is called dynamic receive focus beam-forming [32].

Grating Lobes:

Constructive interference is relied upon to create a focused beam from an array transducer, both during transmit and receive. However, if the spacing of array elements is not fine enough, undesired constructive interference can occur in the imaging field. The result of this interference is referred to as grating lobes, and occurs when the path difference between two adjacent elements is an integer multiple of the pulse wavelength. (Figure 2.19) [35].

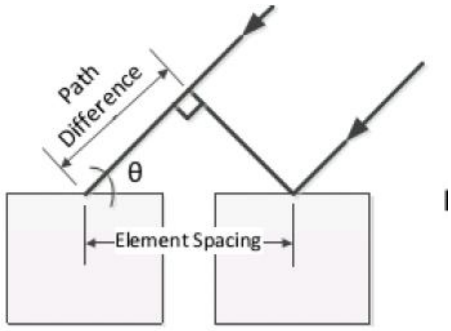

Figure 2.19: Approximation of path difference as related to element space [35]

$$path \cdot difference = elements \cdot spacing * \cos(\theta) \qquad \text{(Eq.2-7)}$$

Any energy coming from a grating lobe is indistinguishable from energy from the actual focal region. This can cause artifacts such as ghosting in the ultrasound image [35].

Grating lobes can occur with any transducer having regularly spaced elements, such as a linear or curvilinear array or a phased array. They are weak replicas of the main beam, at substantial angles (up to 90°) on each side of it (Figure 2.20) [12].

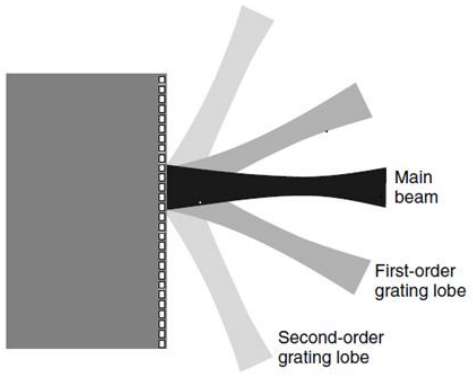

Figure 2.20: Grating lobes [12]

Reducing the spacing further to half a wavelength is required to completely eliminate their effect [35].

2.4.6 US Transducers

A transducer is any device that converts one form of energy into another. An ultrasound transducer converts electrical energy into ultrasound energy and vice versa. Transducers for ultrasound imaging consist of one or more piezoelectric crystals or elements. However, imaging is often preformed with multiple-element “arrays” of piezoelectric crystals [12].

Piezoelectric Effect:

The piezoelectric effect is exhibited by certain crystals that, in response to applied pressure, develop a voltage across opposite surfaces [36, 3٧]. This

effect is used to produce an electrical signal in response to incident ultrasound waves. This deforming effect, termed the converse piezoelectric effect, is used to produce an ultrasound beam from a transducer [15].

Transducer Design:

The piezoelectric crystal is the functional component of an ultrasound transducer. A crystal exhibits its greatest response at the resonance frequency. The components of an ultrasound transducer as shown in (Figure 2.21, Table 2.3) [15]

Table 2.3: The different components of an US transducer [9]

Component	Description
Piezoelectric component	Oscillates at high frequency when AC voltage is applied and develops voltage when pressure (sound waves) is applied to it. The component is often a crystal, but polymers also exist.
Damping material	Absorbs and scatters waves travelling backwards from the piezoelectric component and damps the oscillation.
Insulated wire	A leading wire connected to the piezoelectric component for conducting energizing and developed voltage from an echo.
Metal housing	Grounded metal casing.
Matching plastic front	Protects the surface of the piezoelectric component and helps to overcome the mismatch in acoustic impedance between transducer and tissue.

Multiple-Element Transducers:

Scanning of the patient may be accomplished by physical motion of a single-

element ultrasound transducer. The motion of the transducer may be executed manually by the sonographer or automatically with a mechanical system [15].

Alternatively, the ultrasound beam may be swept back and forth without the need for any mechanical motion through the use of transducer arrays. Transducer arrays are composed of multiple crystals that can change the direction or degree of focus of the ultrasound beam by timing the excitation of the crystals. A common type of transducer is the linear array, or its curved version – the curvilinear array and phased array as shown in (Figure 2.22) [12].

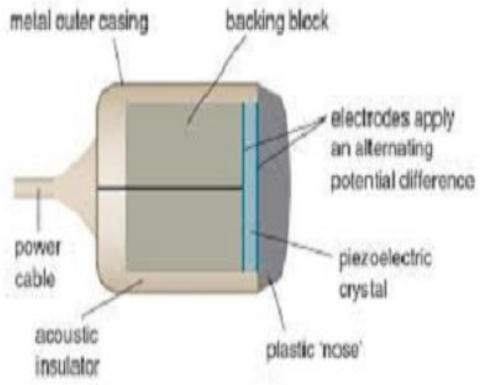

Figure 2.21: Ultrasound transducer components [15]

Figure 2.22: Common ultrasound transducer types [38]

Linear (or curvilinear) transducer:

A common type of transducer is the linear array, or its curved version – the

curvilinear array. Linear arrays offer a rectangular field of view (Figure 2.23) that maintains its width close up to the transducer face and are therefore particularly suitable when the region of interest extends right up to the surface (e.g. neck or limbs). Curvilinear arrays work in the same way as linear arrays, but differ in that the array of elements along the front face forms a curve, rather than a straight line. They share the same benefit of a wide field of view at the surface, but have the additional advantage that the field of view becomes wider with depth. They are therefore popular for abdominal applications, including obstetrics. However, in order to maintain full contact, it is necessary to press the convex front face slightly into the patient [12].

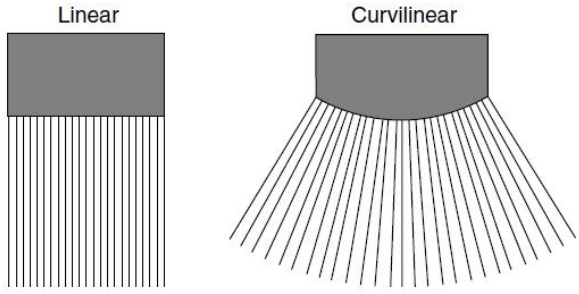

Figure 2.23: Linear and curvilinear scan format [12]

A linear (or curved) array of crystal elements is shown in (Figure 2.23). The crystals, as many as 60 to 240 or more, are excited by voltage pulses in groups of three up to 20 or more. Each excitation of the crystal group results in a "scan line". To obtain the succeeding scan line, the next crystal group is defined to overlap the first as shown in the next figure. This pulsing scheme is referred to as a linear switched array. By sequentially exciting the entire array, an image composed of a number of scan lines (typically 64, 128, 256, etc.) is obtained [15].

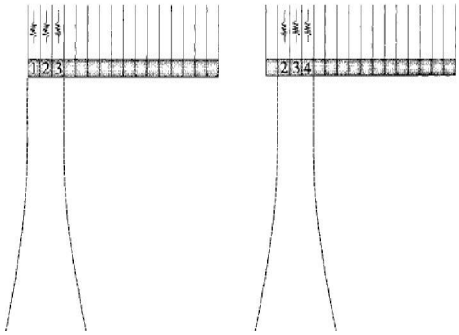

Figure 2.24: Electronic scanning with linear switched array [15]

Phased-array transducer:

The phased-array transducer produces a 'sector' scan format in which the scan lines emanate in a fan-like formation from a point in the centre of the transducer face (Figure 2.25). As with all types of scanner, each scan line represents the axis of a transmit receive beam [12].

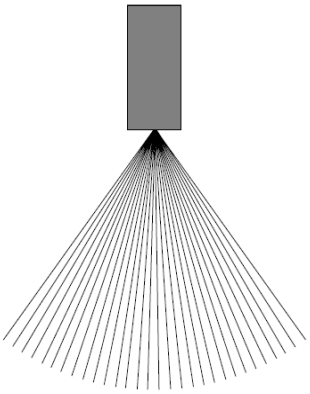

Figure 2.25: Linear and curvilinear scan format [12]

Another method for scanning with a linear array uses phased-array technology. A phase array uses all (typically 128) of the elements of the array to obtain each scan line. By using slight delays between excitations of the elements, the beam may be "swept" to the left or right (Figure 2.26).

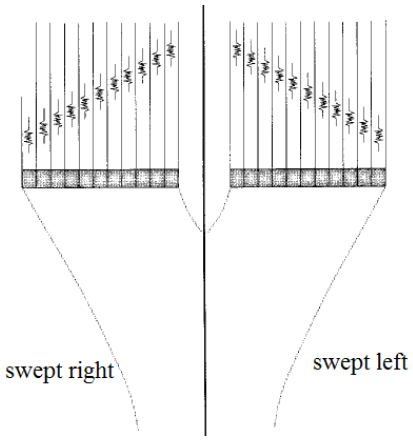

Figure 2.26: Electronic scanning with a linear phased array [15].

A variation in the time delay scheme in a phased array may also be used to focus the beam at various distances throughout each image. In this technique, called dynamic focusing, part of the image is acquired with the focal zone near the transducer face, and part is acquired with the focal zone farther from the transducer face. Thus, two or more images taken at different focal zones may be combined to produce a single image with better axial resolution [15]

2.4.7 Some US image artifacts

Although pixel values in ultrasound images are influenced by fundamental properties such as acoustic impedance and physical density, each pixel value is determined by interrelationships among surrounding materials that are too complex to unfold quantitatively. However, these interrelationships sometimes create artifacts that are recognizable in a qualitative sense [15].

Artifacts of Attenuation, Strong Reflectors (Bone, Stone, and Air) [38]**:**

- **Bone (or Stone) Interface:**

When the US wave strikes bone (and stone), most of the waves are reflected back thus there will be an area of intense hyperechogenicity (whiteness) at the soft tissue-bone interface. Because the surface of bone is often smooth, there is little scattering of the US wave and a clear-cut is produced beyond the reflector. As shown in (Figure 2.27).

- **Air Interface**

On the other hand, soft tissue-air interfaces are more variable in their degree of reflection with some of the US waves incompletely moving through the air-filled structure; thus reverberations occur distal to the air interface creating a "dirty shadow". As shown in (Figure 2.28).

Figure 2.27: Clean shadow. The smooth surface of the cystourolith (urinary bladder stone) generates the clean shadow [38]

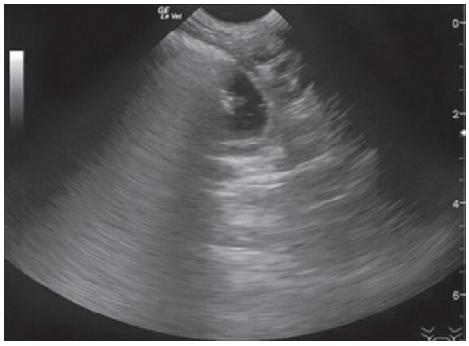

Figure 2.28: Dirty shadow. A gas bubble within a fluid-filled distended loop of small bowel generates a dirty gas shadow because some US waves pass through the structure [38]

Artifacts of Attenuation (Fluid-Filled Structures) [38]:

- **Edge Shadowing (Fluid-Filled Structures)**

When the US waves strike the edge of a fluid-filled structure with a curved surface, such as the stomach wall and urinary bladder, US waves change velocity and bend, resulting in the physical process of refraction. As a result, a thin hypoechoic (darker) to anechoic (black) area lateral and distal to the edge of the curved structure is formed, as illustrated in (Figure 2.29).

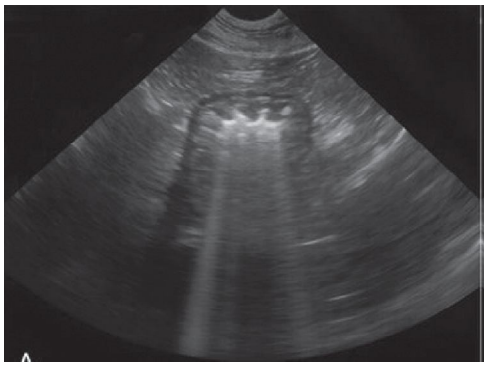

Figure 2.29: An edge shadow artifact is seen arising from the curved edge on the left side of the stomach wall in this image, [38]

Artifacts of Velocity or Propagation [38]**:**

Mirror Artifacts (Strong Reflector [Air]):

When we image a structure that is close to a curved, strong reflector such as the diaphragm, a sound beam can reflect off the curved surface, strike adjacent tissues, reflect back to the curved surface, and then reflect back to the transducer. Because the processor only uses the time it takes for the beam to return home and cannot "see" the ongoing reflections, it will be fooled into placing (mirror) the image on the far side of the curved surface. (Figure 2.30).

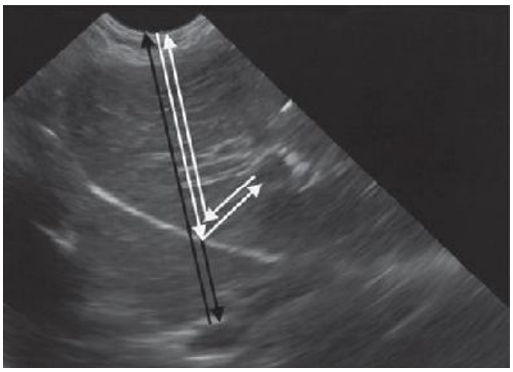

Figure 2.30: Gallbladder appearing to be on both sides of the diaphragm is the classic example of mirror artifact, created by a strong soft tissue-air interface. [38]

CHAPTER THREE
3. LITERATURE REVIEW

The ultrasound beam-former realigns the received signals in order to produce B-scan lines. The method used to realign the signals, and the accuracy with which it can be performed, affects the quality of images obtained from the system. The primary method of realigning the signals is called the Delay and Sum method (DAS). This simply refers to the process of delaying the signal from each channel, and summing them together. There are many different electronic implementations that have been developed in order to realize a DAS beam-former. Here in this section we, will review the common types of beam-formers, and compare the strengths and weaknesses of each design.

Throughout most of the 30 years of real time imaging, analog beam-formers have been the mainstay of all instruments [39]. The common methods for the implementation of analog beam-former for linear/curved arrays and phased arrays will be reviewed and the distinguishing characteristics identified. At the present time the industry is undergoing a major shift to- ward digital beam-formation with the introduction of several commercial systems, given that the earliest digital systems were available roughly 15 years ago [39].

3.1 Analog Beam-forming

Methods in this category use analog beam-former technology (The time delays required for beam-forming have been accomplished by analog delay lines).

“A paper describes electronic sector scanning for ultrasonic diagnosis in 1968, [40]”

The mechanical B-scan used in medical diagnosis has the main disadvantage that it does not provide instantaneous and continuous pictures as the A-scan does in the one-dimension case. In this paper is described the development of an electronic sector scanning equipment especially for medical purposes. By means of a 21-element array sound pulses can be transmitted in every direction within a sector of 90^0. This sector can be scanned at a repetition rate of about 30scans/s.

“A paper represents Improved Image Quality and Clinical Usefulness in 1970, [41]”

During the past year of clinical evaluation, several modifications have been made to the two-dimensional, real time, high resolution ultrasound imaging system known as the Thaumascan system. These modifications were designed to improve the final image quality as well as to enhance the clinical usefulness of this imaging system in assessing various cardiac disorders.

“A paper illustrates a New Ultrasound Imaging Technique Employing Two-Dimensional Electronic Beam Steering in 1974, [42]”

In recent years, ultrasound imaging based on B-mode echosonography has become an accepted and useful technique in medical diagnosis. However, the application of this technique has been limited by the time required to obtain an adequate image, the resolution that can be obtained in the image and problems related to the dynamic range of the echo information. A new ultrasound

imaging system which removes or substantially reduces many of these limitations has been developed in the hope that ultrasound tomography may find even more widespread application and greater diagnostic value.

“A paper introduces clinical results of real-time ultrasonic scanning of the heart using a phased array system in 1977, [43]”

This report describes the operating characteristics and initial clinical results of a new echocardiographic system that produces real-time, high resolution, cross-sectional images of the heart. This system relies upon phased-array principles to rapidly steer and focus the ultrasound beam through the cardiac structures under investigation. A hand-held, linear array of 24 transducers is manipulated on the patient's chest to direct the interrogating plane at various cardiac structures. Images of high line density are presented in selectable sector arcs to a maximum of 90 degrees. This imaging system has been used clinically in over 2,000 patients in the past two and one-half years. Its use in the detection of altered states of ventricular and valvular pathology has been described.

The earliest phased array beam-formers were developed in the late 1960's for imaging of the brain [39] and in the early 1970's for echocardiography [40, 41 and 42] and for obstetrics and gynecology. These early systems involved relatively simple implementations of the beam-former functions. With some of the linear array designs, no focusing was included: they relied completely on using a collimated beam and the narrowing of the beam-shape at the near-to-far field transition. Several significant limitations are immediately apparent. For example, the focal region is quite limited; the side lobe levels are quite

high. The need to suppress side-lobes in clinical imaging was recognized early by using apodization technique as will be described on [44, 45, 46 and 47]. This performance can be dramatically improved by the introduction of apodization or weighting of the transmit pulses and/or received echoes by an appropriate weighting functions. Reports on this came out in the literature in the late 70's. These processing steps became available in commercial instruments starting from about 1980 and onwards [39].

“A paper describes near-field, transient acoustic beam-forming with arrays in 1978, [44]”

For arrays excited with short pulses, the radiation pattern can be significantly different from the pattern with narrow band radiation familiar in optics and radar. Three-dimensional plots of pressure as a function of time and space are shown based on a theory valid in the near-field as well as far-field. Specific results are given for a two-cycle pulse transmitted from arrays with fully sampled apertures and from arrays under-sampled by a factor of four (at 2ʎ spacing) with elements 0.5ʎ and 1.75ʎ wide. Waveforms are shown for unfocused and focused transducers. Special attention is given to the side-lobes and the effects of amplitude weighting the transducer.

“A paper represents flexible real- time system for experimentation in phased-array ultrasound imaging in 1980, [45]”

An experimental phased-array ultrasound imaging system using C3D electronic lenses is being developed in the CIEM at Stanford. This real-time system is designed to extend the imaging capability of the phased array systems used in modern clinical practice. The general purpose machine uses a

modular architecture with a very high degree of computer control of important system variables. The flexibility of this system allows the experimenter great latitude in testing imaging schemes. The machine is comprised of five major computer controlled modules.

"A paper illustrates a phased array acoustic imaging system for medical use in 1980, [46]"

An experimental linear phased array acoustic imaging system has been developed for cardiac, obstetric, and radiological use. This is a real time, pulsed B scan system using either a 2.5 MHz or a 3.5 MHz hand held transducer. The display format is a sector scan with dimensions of 90° × 24 cm and the system is dynamically focused. The system uses an analog heterodyne architecture to greatly simplify the electronics for a densely packed array and to allow use with transducers of different frequencies. With a 20 mm aperture segmented into 64 elements, at 2.5 MHz, the system achieves a 6 dB resolution at 7 cm in water of 2.5 mm in azimuth, 1 mm in range, and 3.5 mm in elevation. Emphasis was put on a system with wide dynamic range; side lobe levels of the array beam plot less than −65 dB have been achieved over the sector. A digital scan converter is used to convert the sector scan to a raster display and for image processing.

"A paper introduces Resolution issues in medical ultrasound in 1985, [47]"

A common figure of merit for imaging systems is resolution –the ability to differentiate two or more closely spaced point targets, when applied to ultrasonic images for medical applications, however, it is not an adequate measure of performance. The clinical user is also concerned with

differentiating subtle textural changes in tissue. We refer to this figure of merit as contrast resolution.

Along with dynamic apodization came the capability to increase the aperture size dynamically during receive, i.e. dynamic aperture. The concept of dynamic focusing with medical ultrasound transducers goes back to the 1950's as described in [47].

When the receive focus advanced, the number of elements in the active receive group is increased. The reason for this comes from the fact that the beam-width at the focus is inversely proportional to the transducer aperture. However, there is no benefit in using a large group when receiving echoes from superficial targets, since elements far from the centre of the group would not be able to receive echoes from them – these targets would be outside the individual receive beams of the outer elements, this is the approach of dynamic receive focusing [12].

A major benefit from dynamic focusing is that, beam-width in the successive focal zones remains fairly constant, keeping lateral resolution as uniformly good as possible at all depths as will be described on [48, 49 and 50].

“A paper describes a digitally controlled CCD dynamically focused phased array in1975, [48]”

This paper presents an electronically focused and linear ultrasonic array using individual CCD delay line chips separately controlled by common digital controller. Use of separate control provides system versatility and accuracy in near field focusing. The system discussed here uses 3.2 cm linear array of 31

ultrasonic transducers at 1.5 MHz's each transducer is provided with a separate transmitter, receiver, and CCD delay line, Outputs from the 31 CCD delay lines are added onto RF summing beams to form the final scanned array beam.

"A paper represents a simplified ultrasound phased arrays sector scanner in 1979, [49]"

The phased array principle was introduced into medical ultrasound by somer and is now mainly used in two-dimensional echocardiography. In a phased array the ultrasound beam is rotated around the transducer and a sector scan is performed. The transducer typically has a width of 1–2 cm and consists of many elements, usually about 30. The rotation of the ultrasound beam is achieved by emitting the ultrasound pulses from the different elements at different instants and subjecting the received echo signals to delays, which are different for each element of the array. The difference in delay τk between adjacent elements is given by Tex where xk is the distance between elements, α is the deflection angle and c is the sound velocity.

"A paper illustrates design of **a** simplified delay system for ultrasound phased array imaging in 1983, [50]"

A novel technique for implementing the dynamically variable delay system, required for electronic sector scanning in ultrasound phased array imaging equipments has been recently introduced. The technique is based on separate and independent processing of the carrier and the envelope of the echo pulses. Carrier phasing is accomplished by electronic phase-shifters, while envelope delay is varied by delay lines, this latter function however, can be performed

using discrete delays in increments much larger than those required by previous techniques. Extensive computer simulations of the array directivity pattern have been performed to evaluate the effect of a coarse delay quantization.

The earliest beam-formers introduced delays through the addition of fixed electrical delay lines in the receive path. Instead delays were often composed of lumped inductor capacitor (LC) circuits. This simple fixed delay structure would not allow for the delay to be varied. In order to improve the performance of the analog beam-former, the fixed delay line was replaced by a tapped delay line (TDL) [51]. A TDL breaks the single long analog delay into small delay sections by using an analog multiplexer (MUX). Digital logic can control the MUX selection. (Figure 3.1) shows the structure of a tapped-delay line analog beam-former.

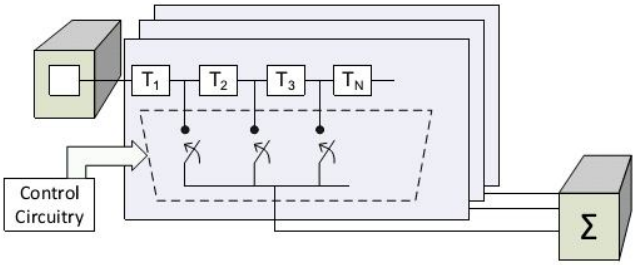

Figure 3.1: A delay line beam-former uses selectable fixed taps to vary the delay on each signal [51]

“A paper introduces a new ultrasound imaging technique employing two-dimensional electronic beam steering in 1973, [51]”

In recent years, ultrasound imaging based on B-mode echo-sonography has

become an accepted and useful technique in medical diagnosis. However, the application of this technique has been limited by the time required to obtain an adequate image, the resolution that can be obtained in the image and problems related to the dynamic range of the echo information. A new ultrasound imaging system which removes or substantially reduces many of these limitations has been developed in the hope that ultrasound tomography may find even more widespread application and greater diagnostic value.

"A paper describes cardiac imaging using a phased-array ultrasound system.1. System-design in 1976, [52]"

A new two-dimensional, real-time, high resolution ultrasound imaging system is described. This system uses a linear array of ultrasound transducers to generate tomographic images of the heart in a circular sector format. Phased array techniques allow rapid steering of the ultrasound beam so that images are produced at the rate of 20 per second, or more, while maintaining a resolution of 2-4 mm throughout the field of view.

In order to accurately beam-form the signals using a TDL, then spacing of delay taps must be equal to the smallest delay step tolerable. This requires a huge amount of hardware, even for small array sizes. The Coarse/fine Analog Beam-former was designed to address these issues. One design is shown in (Figure 3.2). This implementation has been used in both commercial and recent research projects [52, 53]. The coarse/fine beam-former divides the delays into a fine delay which is most commonly provided by a phase shift, rather than a true delay and a coarse delay made up of larger TDL sections.

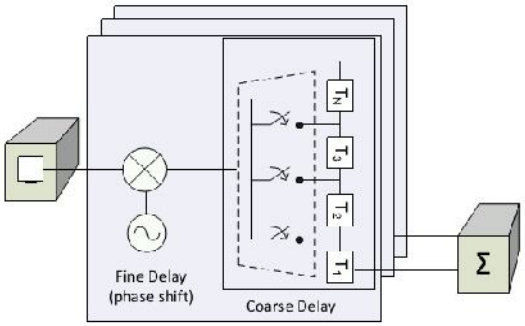

Figure 3.2: A coarse/fine delay beam-former uses fixed taps for coarse adjustment along with a phase shift for fine adjustment [53]

"A paper represents integrated circuit for high-frequency ultrasound annular array in 2003, [53]"

An integrated circuit capable of focusing a high-frequency ultrasound annular array is presented. It uses novel unit-delay architecture to accomplish focusing of the array with a single control voltage. System measurements for a 5-element array indicate excellent pulse fidelity with a dynamic amplitude range of 60 dB at 50 MHz this is the highest frequency single-chip ultrasound beam-former that has been demonstrated to date.

Analog beam-former technology was used in traditional ultrasound systems, in its time delays required for beam-forming can be accomplished by analog delay lines; these analog delay lines impose significant limitations on the beam-former performances, e.g. limited focusing accuracy, and susceptibility to changes in value over time and temperature; because of that at the present time the industry is trend toward digital beam-formation .

3.2 Digital Beam-forming

Most modern US systems convert the analog signals received from the transducer into a digital form before beam-forming. After conversion, beam-forming can then be handled using digital logic.

While the earliest commercially available digital beam-former were available in the early 80's. They did not begin to have a significant impact until the early 90's. Much of this delay was due to the need for ADC converters with sufficiently large number of bits and a high enough sampling rate, an obviously important topic is the number of bits required for ADC conversion. Today the rate of transfer to digital processing is gaining ,momentum, although due to some of the costs associated with the required components, most of the digital systems tend to be high end machines [39].

Existing digital beam-forming techniques can be categorized into two classes, namely time domain beam-forming or frequency domain beam-forming. These classes relate to the domain that the echoed image data is processed or operated on [54]. Here we focus on time domain beam-forming because it is what we use in our project.

3.2.1 Digital Beam-former basics:

The functions of a beam-former include the following [55]:

- Generate transmit timing and possible apodization (the term apodization will be used as a synonym for weighting, tapering and shading) during transmit.
- Supply the time delays and signa1 processing during receive.
- Supply apodization and summing of delayed echoes.

- Possible additional signal processing related activities.

The goal of all of these functions is to create a narrow, uniform beam with low side-lobes over as long a depth as possible. (Figure 3.3) demonstrates the geometry that is usually used.

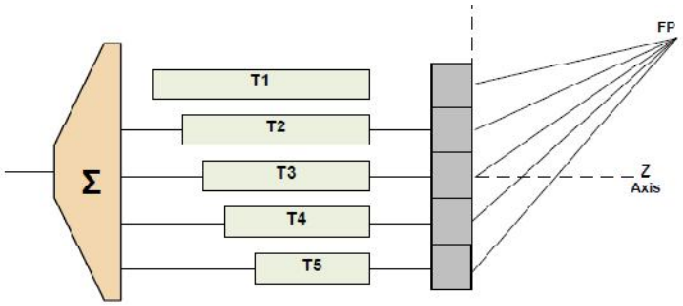

Figure 3.3: Basic geometry for beam-former calculations [55]

(Figure 3.3) also illustrates the reception process. Wave-fronts are shown emanating from a point source labeled as FP. These signals are received by the array elements, amplified and passed on to the delay lines. The delay lines are shown as rectangular boxes whose length corresponds to the desired delay. Finally, the echoes are passed on to the apodization/summer stage, which takes the contributions from each element, multiplies them with a weighting function, and adds up the results. The general expression for the received echo r (t) [56]:

$$r(t) = \sum_{i=1}^{N} A_{ri} \sum_{j=1}^{N} A_{xj} S(t - \tau_{ri} - \tau_{xj} + \frac{2R_{fp}(t)}{C}) \qquad \text{(Eq.3-1)}$$

In this expression, the transmitted wave-shape is *S* (t). The A's refer to whatever weighting function that might be applied to each of the channels during transmitting and receiving operations. In the simplest case these would

be equal to one for uniform aperture weighting. $2R_{fp}$ (t) is the distance of the source point (FP) from the center of the transducer array and c is the velocity of the wave-front in meters per second. Similarly, τ is refer to transmitting and receive delays applied during transmit and receive beam-formation operations. i and j are indices of the receive and transmit elements, respectively, and subscripts r and x refer to receive and transmit operations. Finally, in Equation 3.1, N is the number of transmit and receive elements and will assumed to be constant.

Recently, digital technology in continuous dynamic focusing and steering has drawn attention because it allows quick and accurate control over the delay time [57]. A new digital beam-forming method, called sampled delay focusing (SDF), has been proposed and analyzed by several authors [59].

In implementation of the digital beam-former in this scheme, it is very important to find a sampling method that has negligible error in getting in-phase and quadrature-phase data of the signals received at each array element, the second-order sampling method has been suggested as being the most suitable for the SDF [58].

“A paper illustrates digital interpolation beam-forming for low-pass and band-pass signal in 1979, [57]”

Digital time-domain beam-forming requires that samples of the sensor signals be available at a sufficient rate to realize accurate time delays for beam steering. For many applications, this input rate, which may be significantly higher than the Nyquist rate required for waveform reconstruction, places stringent requirements on A/D converter hardware and transmission cable

bandwidth. Recently, a technique referred to as digital interpolation beam-forming was introduced which greatly relaxes the sampling requirement and provides substantial hardware savings through more flexible design options. This paper extends this work by examining the relationship between interpolation and beam-forming for the important class of "band-pass" signals. Beam-former implementations are presented which utilize these bandwidth-sampling techniques in conjunction with interpolation and which compute beam output points at the generally low rate dictated by the signal bandwidth. The interpolation beam-former achieves time-delay quantization (beam-steering accuracy) independent of both the input and output sampling rates. This approach generally requires less hardware than conventional procedures.

“A paper introduces a New System for Real-Time Synthetic Aperture Ultrasonic Imaging in 1988, [58]”

The synthetic aperture imaging technique has become popular in the field of ultrasonic imaging, but the image reconstruction process takes too long to be applied in practical applications. The authors contrived a new way to generate in real time a cross-sectional image of an object with uniformly high resolution based on the synthetic aperture focusing technique (SAFT). An imaging system was built accordingly that produced a cross-sectional image composed of an assembly of line images of depth direction, i.e., processed A-scan images, and displayed as a scroll picture on a cathode ray tube (CRT), it takes only 3 ms from the start of transmission of the ultrasonic wave to the completion of a line image reconstruction, and the framed image on a CRT is updated at the TV rate of 1/30 S.

The resolution of all imaging systems is limited by the effective aperture size over which data can be collected to reconstruct an image. In the conventional imaging technique, i.e., pencil-beam scanning, the effective aperture size is limited by the physical aperture used for the data collection. There are some limitations in fabricating and controlling the large physical aperture to improve the resolution. The synthetic aperture imaging technique was developed to overcome this disadvantage in the conventional imaging technique. However, a large number of calculations are inevitable for synthetic aperture imaging.

"A paper describes synthetic aperture imaging with a virtual source element in 1996, [59]"

Currently ultrasonic imaging is performed in one of two modes: conventional B-scan imaging with a focused transducer or array imaging using beam-forming processing to achieve the focus. Conventional B-mode imaging suffers from a limited depth of focus while synthetic aperture imaging is limited by a low signal to noise ratio (SNR). A new technique has been proposed [61] that combines these two techniques to overcome the limited depth of focus. The new technique involves focusing the region beyond the focus of the transducer by considering the focus a virtual element. In this paper, the use of the focus as a virtual element is examined. Using data collected with tungsten wires in a water-bath, it was found that resolution comparable to the resolution at the focus could be achieved while obtaining an acceptable SNR. Apodization was found to lower the side-lobes, but only at the expense of lateral resolution.

A basic limitation of conventional B-mode imaging is that lateral resolution depends on the depth in the image. In 1996, Passman and Ermert introduced a technique to overcome this resolution limitation. The new technique involved treating the focus of the transducer as a virtual source for synthetic aperture (SA) processing. In their formulation, the virtual source was assumed to produce approximately spherical waves over a certain aperture angle. This study examines the ability of known SA techniques to improve the quality of images created with a virtual source element [60].

“A paper represents sparse array imaging with spatially encoded transmits in 1997, [61]”

The frame rate in medical ultrasound imaging may be increased significantly by reducing the number of transmit firings per image frame. Cooley et al. [62] and Lockwood et al. [63] have described synthetic aperture imaging systems where each frame is imaged using data obtained from a small number of transmit elements fired in succession. These "synthetic transmit aperture" systems have potential for very high frame rates, but they also suffer from low SNR. In this paper we present a method for increasing the SNR of such systems by using spatially-encoded transmits. The transmitted power is increased by having multiple active transmitters in each firing. The active transmitters are encoded in a spatial code which allows the received data to he subsequently sorted by each transmitter for synthetic aperture beam-forming.

In conventional ultrasound imaging systems, each firing transmits a focused beam at a particular focal position. The beam is scanned across the imaging area in a succession of firings to generate a single image frame. The frame rate

may be increased significantly by reducing the number of transmit firings per image frame. In order for a smaller number of transmit firings to cover the same area as before, the transmit beam-width for each firing must get broader. To avoid the broader transmit beam from degrading the round-trip beam, the transmit aperture is synthesized over multiple transmits [63].However, low SNR is a major problem faced by such systems. While generally called synthetic aperture (SA), we further categorize it into "synthetic transmit aperture" (STA) when only the transmit locations change and "synthetic receive aperture" (SRA) when only the receive locations change [64].

“A paper illustrates synthetic focus imaging using partial datasets in 1994, [62]

Synthetic focus is method of constructing images from the signals associated with each pair of transmit/receive elements of a two-way transducer array. Using conventional aperture designs, synthetic focus datasets contain significant redundancy. By replacing the two-way imaging system with a one-way array of virtual elements, complete subsets of the synthetic focus dataset can be readily identified. These techniques can also be used to significantly reduce the data acquisition requirements for synthetic focus imaging, leading to the possibility of very high frame rate imaging.

“A paper introduces design of sparse array imaging systems in 1995, [63]”

A method for designing sparse periodic arrays is described. Grating lobes in the two way radiation pattern are avoided by using different element spacing’s for transmission and reception. The transmit and receive aperture functions are

selected such that the convolution of the aperture functions produces a desired effective aperture. Here, we apply the effective aperture method to the design of a sparse array for a very high frame rate (1000 images/s) imaging system. The high frame rate is achieved by using synthetic aperture beam-forming utilizing only a few transmit pulses for each image. To compensate for the resulting loss in signal, the power delivered to each transmit element is increased and multiple transmit elements are used for each transmit burst.

"A paper describes real-time synthetic receive aperture imaging: experimental results in 1994, [64]"

Improvements in medical ultrasonic image resolution are typically accompanied by significant increases in the number of piezoelectric array elements and beam-former channels. The synthetic receive aperture (SRA) imaging technique achieves dramatic improvements in effective beam-former channel count without concomitant increases in system cost and complexity. We have constructed a real-time SRA imaging system which forms images using a fully sampled 128 element array with a 128 channel transmit beam-former, but only a 32 channel receive beam-former. We describe this system and present initial experimental results.

"A paper represents modular FPGA-based digital ultrasound beam-forming in 2011, [65]"

The evaluation of ultrasound system is measured by the development in analog and digital electronics. A modular field programmable gate array (FPGA)-based digital ultrasound beam-forming is presented. The digital

beam-forming is implemented in Virtex-5 FPGA. The objective of this work is to develop a modular low-cost PC-based digital ultrasound imaging system that has almost all of its processing steps done on the PC side. The system consists of: two 8 channels block and reconstructed line block. The 8 channel block consist of: memory block to save the samples data after converted to fixed point type, delay block implemented by addressable shift register - the delay process is based on sampled delay focusing (SDF) - and M-code block applied the summation of each RF channel samples. The reconstructed block consists of pipelined adder to apply the summation of the two 8 channels blocks. The power consumption and device utilization was acceptable. Also it is possible to build 16, 32, 64 and 128-channel beam-former. The hardware architecture of the design provided flexibility for beam-forming.

"A paper illustrates digital signal processing methodologies for conventional digital medical ultrasound imaging system in 2013, [2]"

Ultrasound imaging is an efficient, noninvasive, method for medical diagnosis. A commonly used approach to image acquisition in ultrasound system is digital beam-forming. Digital beam-forming, as applied to the medical ultrasound, is defined as phase alignment and summation of signals that are generated from a common source, by received at different times by a multi-elements ultrasound transducer. In this paper first: we tested all signal processing methodologies for digital beam-forming which included: the effect of over sampling techniques, single transmit focusing and their limitations, the apodization technique and its effect to reduce the side-lobes, the analytical envelope detection using digital finite impulse response (FIR) filter approximations for the Hilbert transformation and how to compress the

dynamic range to achieve the desired dynamic range for display (8 bits). Here the image was reconstructed using physical array elements and virtual array elements for linear and phase array probe. The results shown that virtual array elements were given well results in linear array image reconstruction than physical array elements, because it provides additional number of lines. However, physical array elements shown a good results in linear phase array reconstruction (steering) than virtual array elements, because the active elements number (Aperture) is less than in physical array elements. We checked the quality of the image using quantitative entropy. Second: a modular FPGA-based 16 channel digital ultrasound beam-forming with embedded DSP for ultrasound imaging is presented. The system is implemented in Virtex-5 FPGA (Xilinx, Inc.). The system consists of: two 8 channels block, the DSP which composed of the FIR Hilbert filter block to obtain the quadrature components, the fractional delay filter block (in-phase filter) to compensate the delay when we were used a high FIR order, and the envelope detection block to compute the envelope of the in-phase and quadrature components. The Hilbert filter is implemented in the form whereby the zero tap coefficients were not computed and therefore an order L filter used only L/2 multiplications. This reduced the computational time by a half. From the implementation result the total estimated power consumption equals 4732.87 mW and the device utilization was acceptable. It is possible for the system to accept other devices for further processing. Also it is possible to build 16-, 32-, and 64-channel beam-former. The hardware architecture of the design provided flexibility for beam-forming.

CHAPTER FOUR

4. METHODOLOGY

This chapter introduces the research methods which are about to develop a tool in MATLAB that should assist students in understanding the necessary processing steps to convert US digital RF data into brightness modulation image. These transformation steps represent only one part of the whole processing pipeline of an ultrasound system. The tool will provide the user with a framework for the processing pipeline. In this project brightness modulation image is reconstructed using physical array elements for linear and phase array probe.

With the growing availability of high-end integrated analog front-end circuits, distinction between different digital ultrasound imaging systems is determined almost exclusively by their software component. Our previous work concerned on description the digital ultrasound imaging system and the processing steps which done on the PC side [2, 65]. A commonly used approach to image acquisition in ultrasound system is digital beam-forming. Digital beam-forming, as applied to the medical ultrasound, is defined as phase alignment and summation of signals that are generated from a common source, by received at different times by a multi-elements ultrasound transducer [65].

The commonly use arrays are linear, curved, or phase array. The important distinctions arise from the method of beam steering use with these arrays. For **linear and curve linear**, the steering is accomplished by selection of a group

of elements whose location defines the phase center of the beam. In contrast to linear and curve linear array, **phase array transducer** required that the beam-former steers the beam with switched set of array elements [65].

These requirements mention important differences in complexity over the linear and curved array [65].

4.1 Block Diagram

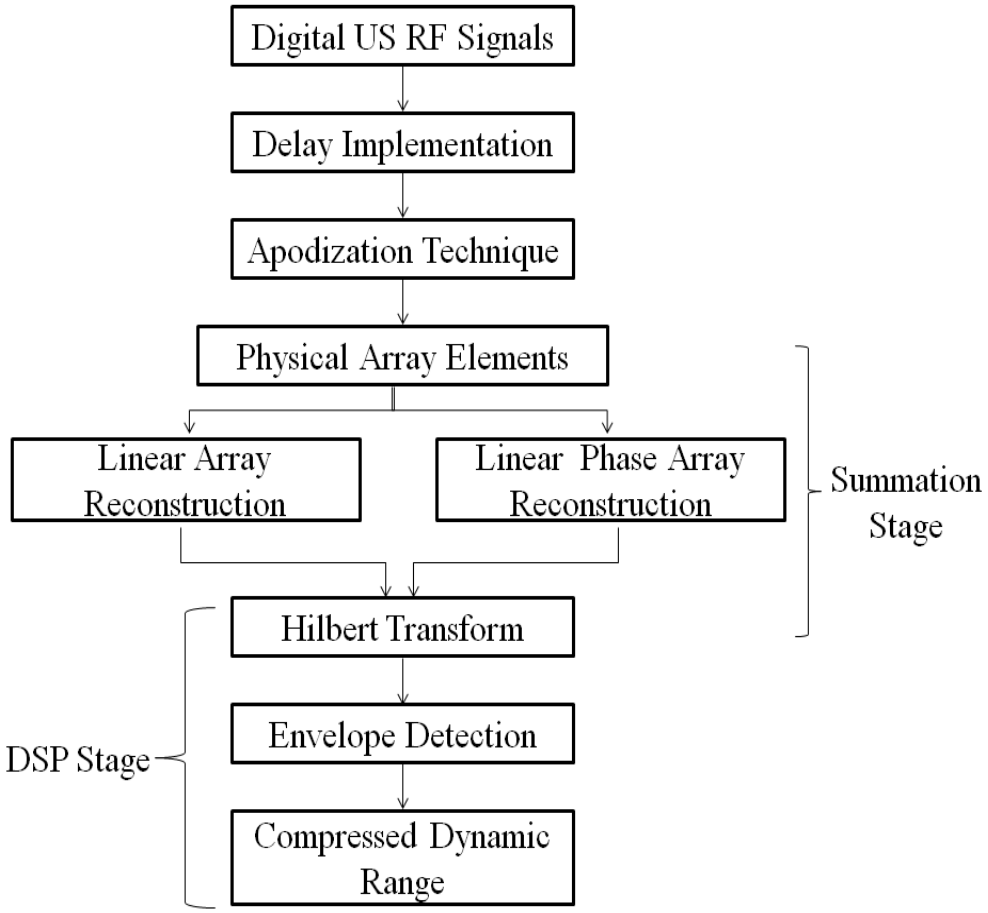

Figure 4.1: Block diagram of proposed method for transform RF data to B-mode image.

4.2 Delay Equation

(Figure 4.2) shows the geometry which is used to determine the channel and depth-dependent delay of a focused transducer array.

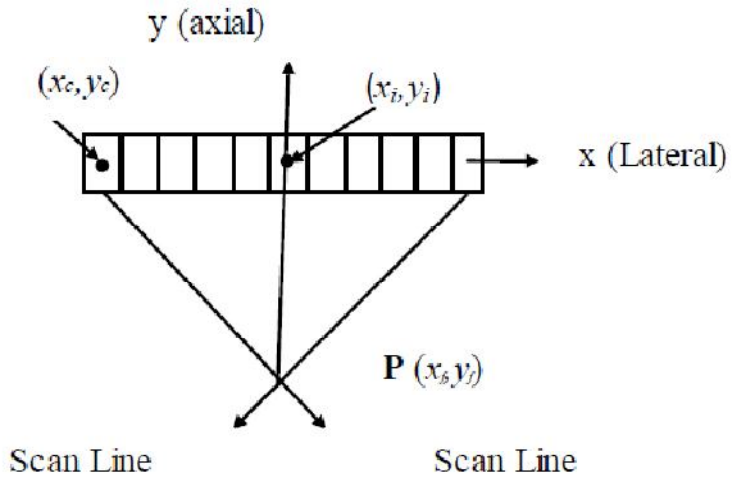

Figure 4.2: Geometry of a focused transducer array [2]

When US wave transmits into the medium an echo wave propagates back from the focal point (P) to the transducer, the distance from P to the origin is equal to the Euclidian distance between the spatial point (x_i, y_i) and (x_f, y_f), so the time takes from p to (x_i, y_i) is given by [66]:

$$t_i = \frac{1}{c}\sqrt{(x_i - x_f)^2 + (y_i - y_f)^2} \qquad \text{(Eq.4-1)}$$

Where (x_f, y_f) is the position of the focal point, (x_i ,y_i) is the center for the physical element number i, and c is the speed of sound. The point (x_c, y_c) is selected to be a reference for the imaging process. The propagation time (t_c) for this was calculated as in equation (4-1), but the distance here from P to the reference (x_c, y_c). The delay which use on each element (t_i) of the array is then calculated using the next equation [66] :

$$\Delta t_i = t_c - t_i \qquad \text{(Eq.4-2)}$$

4.3 physical Array Elements

4.3.1 Linear Array Reconstruction

Scan plane focusing in transmission:

Since the cylindrical lens does nothing to reduce the beam-width in the scan plane, an electronic method of focusing must be provided, if good lateral resolution is to be achieved. This is controlled by the operator, who sets the transmission focus at the depth for which optimum lateral resolution is desired. This ensures that the transmission beam is as narrow as possible there (the receive beam must also be narrow there). Pulses from all the elements in the active group must arrive at the transmission focus simultaneously in order to concentrate the power into a narrow 'focal zone'. However, the distance between an element and the focus, which lies on the beam axis passing through the centre of the group, is slightly, but crucially, greater for the outer elements of the group than for more central elements. Pulses from elements further from the centre of the active group must, therefore, be transmitted slightly earlier than those nearer the centre (Figure 4.3). At points outside the required focal zone, the individual pulses from different elements arrive at different times, producing no more than weak acoustic noise. [12].

Scan plane focusing in reception:

As in the case of transmission focusing, allowance must be made for the fact that the distance between the required focus and a receiving element is greater

for elements situated towards the outside of the group than for those near the centre. This is done by electronically delaying the electrical echo signals produced by all transducer elements except the outermost, before summing them together (Figure 4.4) [12].

The delays are chosen such that the sum of the travel time as a sound wave (from the focus to a particular element) plus the delay imposed on the electrical echo signal is the same for all elements. This means that the imposed electronic delays are greater for elements closer to the centre of the active group, for which the sound wave travel times are least [12].

In this way, the echo signals are all aligned in phase at the summing point and a large-summed signal is obtained for echoes from the desired receive focal zone, but only a weak-summed signal (acoustic noise) results from echoes from elsewhere [12].

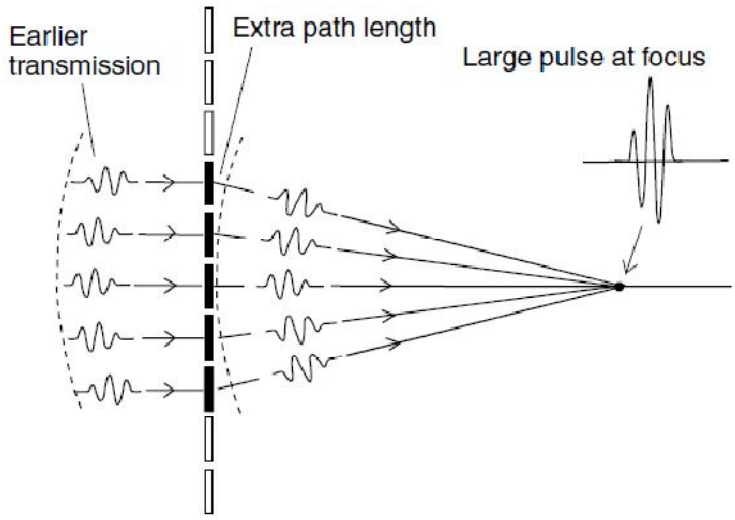

Figure 4.3: Creating transmission focus for a linear array transducer [12]

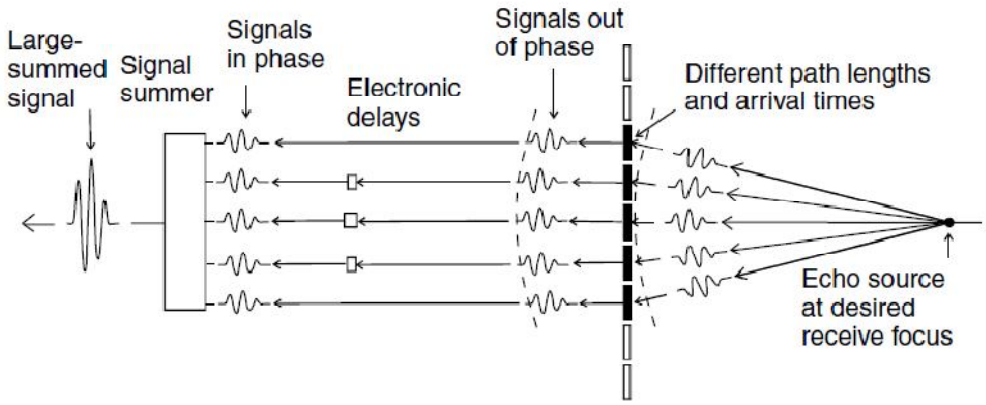

Figure 4.4: Creating receive focus for a linear array transducer [12]

Selected of a group of elements (aperture) whose location is defines the phase center of the beam [66], electronic focusing was applied on receive for each aperture. Received at the aperture elements are delayed by focusing delays and summed to form scan line in the image. After that one elements shift is applied to the aperture and the process was repeated till the end of the array elements at the outer side processing all image scan lines (Figure 4.5 where aperture equal 16 elements). The number of lines is equal to the total number of elements minus the number of the aperture elements plus one [65].

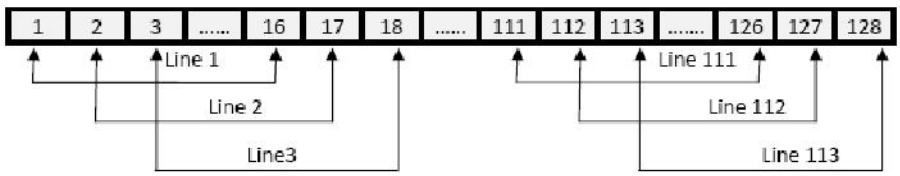

Figure 4.5: Physical linear array elements [65]

Here the delay values were calculated based on the previous equations (Eq. 4-1 and 4-2) and specifications of the probe which has been used to collect the RF data that was used in the project.

Also we reconstruct the image using aperture equal to 4, 8, 16, 32 and 64 to compare between them.

4.3.2 Linear Phase Array Reconstruction

Similar signal-delaying techniques to those previously described for linear-array transducers are used to achieve focusing of transmit and receive beams in the scan plane [12].

Scan plane focusing (and steering) in transmission

As described previously for linear-array transducers, focusing in transmission requires that pulses from all the elements arrive simultaneously at the transmission focus. The early starts needed by each element can be pre-calculated by the manufacturer for each possible position of the transmission focus along the various scan lines (Figure 4.6).

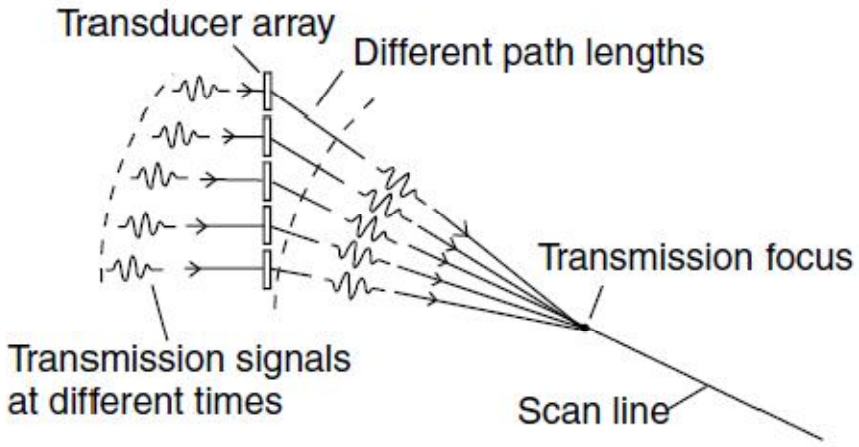

Figure 4.6: Creating transmission focus for a phased array transducer [12]

Scan plane focusing (and steering) in reception

Similarly, in reception, carefully pre-selected electronic delays are used to ensure that an echo from a desired receive focus takes the same time to reach the signal summer, irrespective of which element is considered (Figure 4.7) [12].

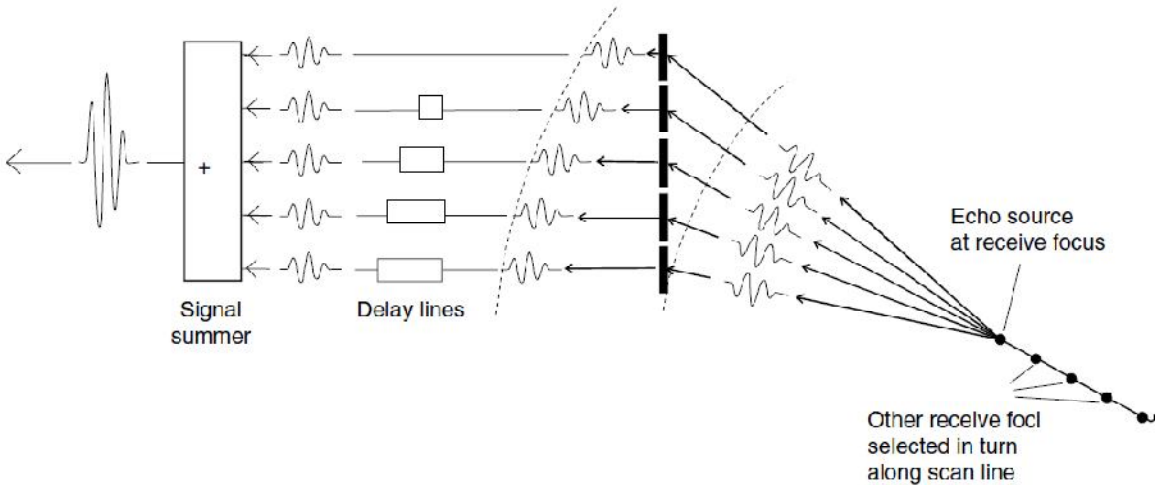

Figure 4.7: Creating receive focus for a phased array transducer [12]

In contrast the linear array, phase array transducer required that the beam-former steered the beam with an un-switched set of array elements [67]. In this process, the time shifts follow a linear pattern across of array from one side to another side. In receive mode, the shifted signals are summed together after phase shift and some signal conditioning to produce a single output. This reconstruction technique divides the field of view (FOV) into different point targets (raster points), *P (i, j)* [2].

Each point represented as an image pixel, which is separated laterally and axially by small distances. Each target is considered as a point source that transmits signals to the aperture elements as in (figure 4.8). The beam-forming timing is then calculated for each point based on the distance *R* between the

point and the receiving element, and the velocity of ultrasonic beam in the media. Then the samples corresponding to the focal point are synchronized and added to complete the beam-forming as the following [2]:

$$p_D(i,j) = \sum_{n=1}^{N} x_n(k_{ij}) \qquad \text{(Eq.4-3)}$$

Where, P_D (i, j) is the signal value at the point whose its coordinates are (i, j), and $x_n(k_{ij})$ is the sample corresponding to the target point in the signal x_n received by the element number n. The sample number k_{ij} which is equivalent to the time delay is calculated using the equation below [2]:

$$k_{ij} = \frac{R_n(i,j)}{T * c} \qquad \text{(Eq.4-4)}$$

Here R_n (i, j) is the distance from the center of the element to the point target, c is the acoustic velocity via the media, and T is the sampling period of the signal data.

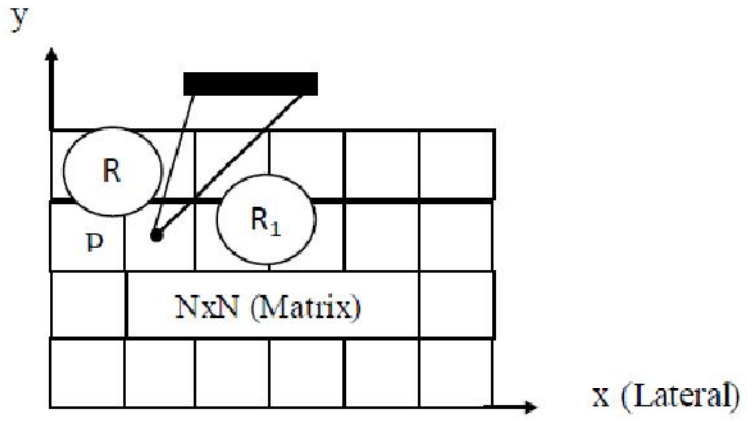

Figure 4.8: Geometry for raster point technique [2]

4.4 Apodization

Another beam-forming process, known as 'apodization', can also be employed. In transmission, this involves exciting the elements non-uniformly in order to control the intensity profile across the beam. For example, if the inner elements are excited more than the outer elements, side lobes can be reduced in amplitude and the focal zone can be extended. Apodization of the receive beam can be achieved by giving different amplifications to the signals from each element (Figure 4.9) [12].

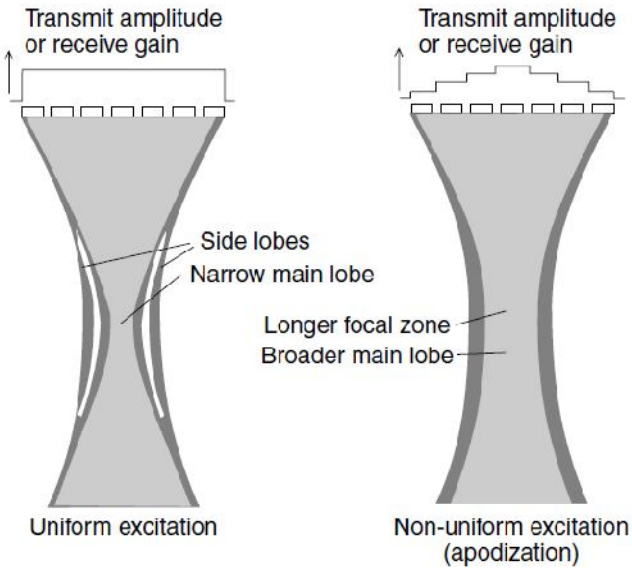

Figure 4.9: Apodization technique in transmit and receive beam [12]

If you look at the next figure of the transmit beam shape you will see there are many weaker beams at each side of the beam, these are called side-lobes. The side-lobes can cause artifacts in the ultrasound image and is therefore not wanted. Apodization is a method to reduce the side-lobes and works by reducing the signal strength on the channels at the edge of the transducer.

(Figure 4.10) shows how the shape of the beam is affected by the apodization. The side-lobes almost completely disappear at the cost of a little wider beam. Apodization is also used with receive beam-forming and is implemented by multiplying the signals from the channels with a windowing function.

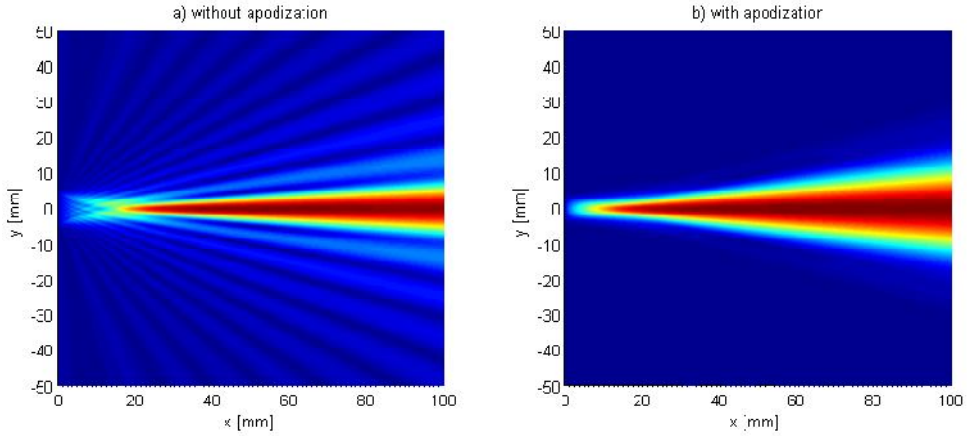

Figure 4.10: Shape of beam with and without apodization [68]

Aperture function needed to have rounded edges that taper toward zero at the ends of the aperture to create low side lobes levels. In this project we use windowing functions (blackman) as apodization functions to reduce the side lobes.

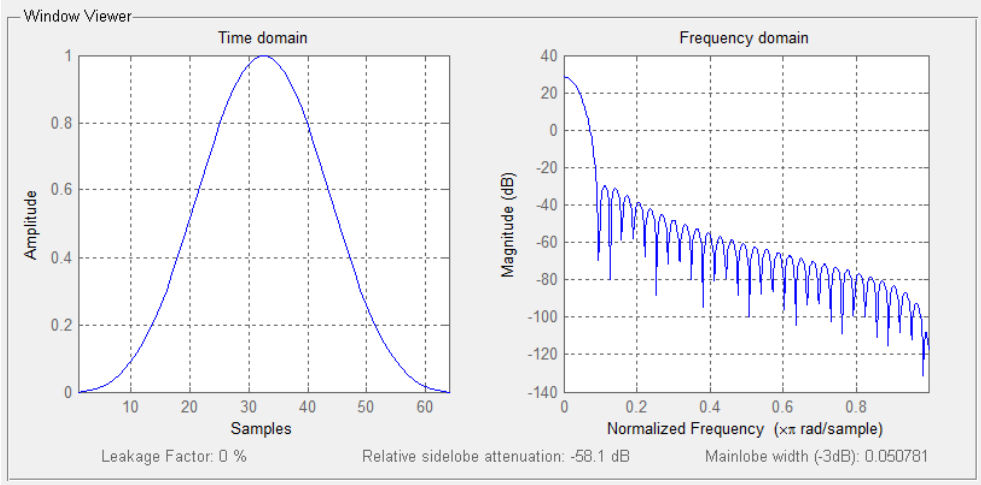

Figure 4.11: 64-length black-man window in time and frequency domain.

We use black-man window according to the information which exists in appendix (As shown in table A), as can be shown the Blackman apodization function has the best SNR, best reduction in the side-lobe and moderate main lobe width compared to the other windows.

4.5 Envelope Detection

After delay and sum, the analytic envelope of the signal is calculated as the square root of the sum of the squares of the real and quadrature components. The most accurate way of obtaining the quadrature components was to pass the echo signal through a Hilbert transform, because it provides 90-degree phase shift at all frequencies [2, 69].

The Hilbert transformation filter acts like an ideal filter that removes all the negative frequencies and leaves all positive frequencies untouched. A number of authors suggested the use of digital FIR filter approximations to implement the Hilbert transformation [2].

4.5.1 FIR Hilbert Transform Filter Design

Digital Hilbert transformers are a special class of digital filter whose characteristic is to introduce a $\pi/2$ radians phase shift of the input signal. In the ideal Hilbert transformer all the positive frequency components are shifted by $-\pi/2$ radians and all the negative frequency components are shifted by $\pi/2$ radians. However, these ideal systems cannot be realized since the impulse response is non-causal. Nevertheless, Hilbert transformers can be designed either as Finite Impulse Response (FIR) or as Infinite Impulse Response (IIR) digital filters, and they are used in a wide number of Digital Signal Processing

(DSP) applications, such as digital communication systems, radar systems, medical imaging and mechanical vibration analysis, and others [69, 70].

IIR Hilbert transformers perform a phase approximation. This means that the phase response of the system is approximated to the desired values in a given range of frequencies. The magnitude response allows passing all the frequencies, with the magnitude obtained around the desired value within a given tolerance. On the other hand, FIR Hilbert transformers perform a magnitude approximation. In this case the system magnitude response is approximated to the desired values in a given range of frequencies. The advantage is that their phase response is always maintained in the desired value over the complete range of frequencies. Whereas IIR Hilbert transformers can present instability and they are sensitive to the rounding in their coefficients, FIR filters can have exact linear phase and their stability is guaranteed. Moreover, FIR filters are less sensitive to the coefficients rounding and their phase response is not affected by this rounding. Because of this, FIR Hilbert transformers are often preferred. Nevertheless, the main drawback of FIR filters is a higher complexity compared with the corresponding IIR filters [70].

For linear time invariant (LTI) a FIR filter can be described in this form [2]:

$$y[n] = b_0 x[n] + b_1 x[n-1] + ... + b_M x[n-M]$$

$$= \sum_{i=0}^{M} b_i x[n-i] \qquad \text{(Eq.4-5)}$$

Where x is the input signal, y is the output signal, M is the filter order and the constants b_i, $i = 0, 1, 2, \ldots, M$, are the coefficients.

Complex signals, analytic signals and Hilbert transformers

A real signal is a one-dimensional variation of real values over time. A complex signal is a two-dimensional signal whose value at some instant in time can be specified by a single complex number. The variation of the two parts of the complex numbers, namely the real part and the imaginary part, is the reason for referring to it as two-dimensional signal. Real signals always have positive and negative frequency spectral components, and these components are generally real and imaginary. Complex signals (known as analytic signals or also as quadrature signals), on the other hand, do not have a negative part neither in their real nor in their imaginary part [70].

The real part and the imaginary part of the analytic signal are related trough the Hilbert transform. In simple words, given an analytic signal, its imaginary part is the Hilbert transform of its real part. (Figure 4.12) shows the Hilbert transform relation between the real and imaginary parts of $x_c(t)$, where $x_c(t)$ is the complex signal, $x_r(t)$ is the real part and $x_i(t)$ is the imaginary part [70].

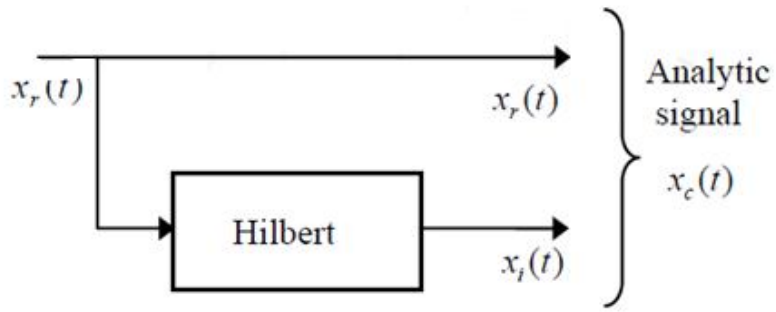

Figure 4.12: Hilbert transform relations between $x_r(t)$ and $x_i(t)$ to generate $x_c(t)$ [70].

The motivation for creating analytic signals, or in other words, for eliminating the negative parts of the real and imaginary spectral components of real signals, is that these negative parts have in essence the same information that the positive parts involve. The elimination of these negative parts reduces the required bandwidth for the processing [70].

The impulse response of the Hilbert filter with length N is defined as [2]:

$$h(n) = \begin{cases} \frac{2}{\pi}\frac{\sin^2(\pi(n-\alpha)/2)}{n-\alpha}, n \neq \alpha \\ 0, n = \alpha \end{cases} \quad \text{(Eq.4-6)}$$

Here we chose filter length equal 24, According to the result which has been accessed in the previous study [2], in that study the normalized root mean square error (RMSE) between the designed FIR Hilbert filter and ideal Hilbert transform filter for filter length equal (16, 20, 24, 28 and 32) was measured, the selected length provided a good result for the qadrature components compared to ideal Hilbert transform filter.

4.6 Compressed the Dynamic Range

After the envelope detection the signal values can be rescaled to fit the grayscale color map in order to display the signals as a B-Mode image. But usually the image will be very dark and structures will be hard to see. This is due to the fact that there are usually some relatively high peaks in the envelope signal corresponding to materials with a very high reflectivity. When rescaling the whole envelope this peaks cause a down-shift of the other values. As a result the image looks dark. To compensate for such peaks the signal

values are not rescaled linearly. There are various possibilities to rescale the image non-linearly. All of them have in common that higher values are more attenuated than lower ones in order to increase the overall brightness while preserving the order of the signal values. One of these methods is to find the logarithm of the envelope signal. Usually the value range is compressed to 8 bits since the ability of the human eye to distinguish grayscale colors is limited anyway. In this project we use Log transformation to compress the dynamic range. The general form of the log transformation is [71]:

$$s = c * \log(1 + r) \qquad \text{(Eq.4-7)}$$

Where, r and s denoted the values of pixels before and after processing (log transformation) respectively, c is a constant. The shape of the log curve in (Figure 4.13) shows that this transformation maps a narrow range of low gray-level values in the input image into a wider range of output levels. The opposite is true of higher values of input levels [71].

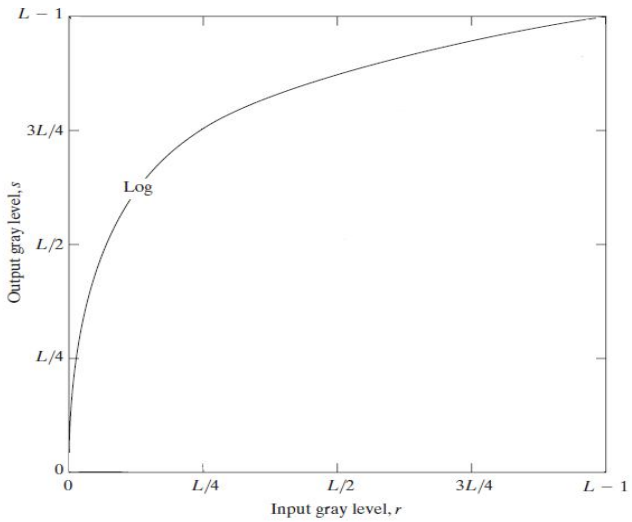

Figure 4.13: Log transformation functions used for image enhancement [71].

Log transformation compressed the dynamic range with a large variation in pixels values [2].

4.7 Graphical User Interface

A graphical user interface (GUI) is a graphical display in one or more windows containing controls, called components that enable a user to perform interactive tasks. The user of the GUI does not have to create a script or type commands at the command line to accomplish the tasks. Unlike coding programs to accomplish tasks, the user of a GUI need not understand the details of how the tasks are performed. Most GUIs wait for their user to manipulate a control, and then respond to each action in turn. Each control, and the GUI itself, has one or more user-written routines (executable MATLAB code) known as callbacks, named for the fact that they "call back" to MATLAB to ask it to do things. The execution of each callback is triggered by a particular user action such as pressing a screen button, clicking a mouse button, selecting a menu item, typing a string or a numeric value, or passing the cursor over a component [72].

GUI components can include menus, toolbars, push buttons, radio buttons, list boxes, and sliders—just to name a few. GUIs created using MATLAB tools can also perform any type of computation, read and write data files, communicate with other GUIs, and display data as tables or as plots [72].

MATLAB is a widely used matrix based equation solving program, which has a Command Window for interactive use and a program editor. It has the features of a general purpose programming language along with a vast

collection of built-in functions which include extensive graphical capability. MATLAB‟s basic **plot** or **plot3** functions generate two or three dimensional graphs of data vectors. Creating Graphical User Interfaces (GUIs) enable interaction with graphical objects such as text boxes and push-buttons [73].

MATLAB GUI can be built in two ways [72]:

- Use GUIDE (GUI Development Environment), an interactive GUI construction kit.
- Create code files that generate GUIs as functions or scripts (programmatic GUI construction).

MATLAB GUIDE:

MATLAB has a built-in Graphical User Interface Development Environment (GUIDE), with which we can lay out the GUI graphically and have MATLAB automatically generate the code [73].

GUIDE tools can be used to [72]:

- Lay out the GUI

Using the GUIDE Layout Editor, you can lay out a GUI easily by clicking and dragging GUI components — such as panels, buttons, text fields, sliders, menus, and so on — into the layout area as shown in the next figure.

- Program the GUI

GUIDE automatically generates an M-file that controls how the GUI operates. The M-file initializes the GUI and contains a framework for all the GUI callbacks — the commands that are executed when a user clicks a GUI

component. Using the M-file editor, you can add code to the callbacks to perform the functions you want them to.

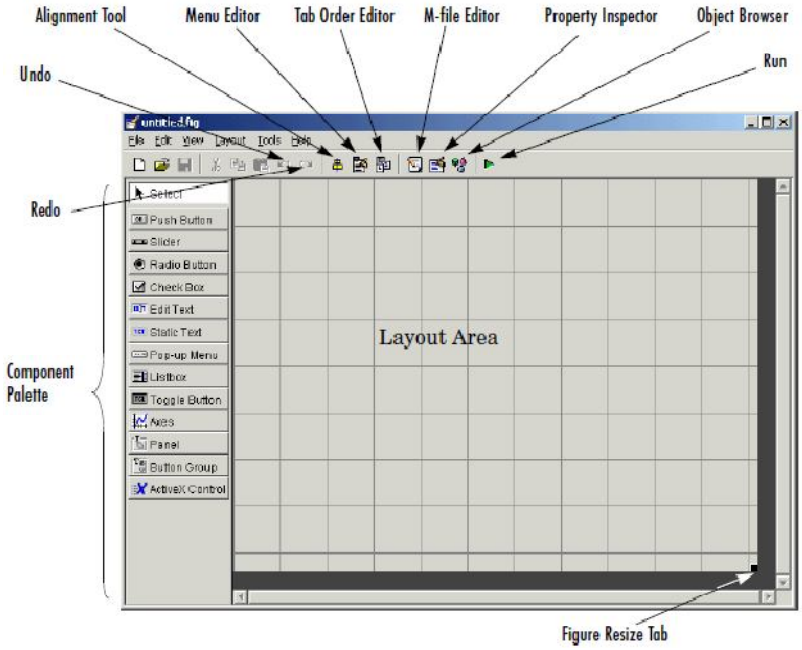

Figure 4.14: GUI template in the layout editor [72]

The component palette at the left of the Layout Editor contains the components that you can add to your GUI such as [72]:

Push Button

Push buttons generate an action when clicked. For example, an **OK** button might close a dialog box and apply settings. When you click a push button, it appears depressed; when you release the mouse, the button appears raised and its callback executes.

Toggle Button

Toggle buttons generate an action and indicate whether they are turned on or off. When you click a toggle button, it appears depressed, showing that it is

on. When you release the mouse button, the toggle button's callback executes. However, unlike a push button, the toggle button remains depressed until you click the toggle button a second time. When you do so, the button returns to the raised state, showing that it is off, and again executes its callback.

Radio Button

Radio buttons are similar to check boxes, but are typically mutually exclusive within a group of related radio buttons. That is, you can select only one button at any given time. To activate a radio button, click the mouse button on the object. The display indicates the state of the button.

Check Box

Check boxes generate an action when checked and indicate their state as checked or not checked. Check boxes are useful when providing the user with a number of independent choices that set a mode, for example, displaying a toolbar or generating callback function prototypes.

Edit Text

Edit text controls are fields that enable users to enter or modify text strings. Use edit text when you want text as input. The String property contains the text entered by the user. The callback executes when you press **Enter** for a single-line edit text, **Ctl+Enter** for a multi-line edit text, or the focus moves away.

Static Text

Static text controls display lines of text. Static text is typically used to label other controls, provide directions to the user, or indicate values associated

with a slider. Users cannot change static text interactively and there is no way to invoke the callback routine associated with it.

Slider

Sliders accept numeric input within a specific range by enabling the user to move a sliding bar, which is called a slider or thumb. Users move the slider by pressing the mouse button and dragging the slider, by clicking in the trough, or by clicking an arrow. The location of the slider indicates a percentage of the specified range.

List Box

List boxes display a list of items and enable users to select one or more items.

Pop-Up Menu

Pop-up menus open to display a list of choices when users click the arrow.

Axes

Axes enable your GUI to display graphics (e.g., graphs and images). Like all graphics objects, axes have properties that you can set to control many aspects of its behavior and appearance.

Panel

Panels group GUI components. Panels can make a user interface easier to understand by visually grouping related controls. A panel can have a title and various borders.

Here in this project we use MATLAB GUIDE to create our GUI which helps us in representing the project result in a simplified manner.

CHAPTER FIVE
5. RESULTS AND DISCUSSION

A new compact educational software tool for digital ultrasound imaging system that has almost all of its processing steps done on the personal computer (PC) side using MATLAB program had been developed.

5.1 Ultrasound Data

The digital ultrasound RF data used in this study were obtained from the Biomedical Ultrasound Laboratory [2], University of Michigan; the phantom data set that was used to generate the results here is under the name "Acusonl7". The parameters for this data set are as follows: the number of channels was 128 channels, and the A/D sampling rate was 13.8889 MSPS. Linear shape transducer was used to acquire the data with center frequency of 3.5 MHz, and element spacing of 0.22mm. Each ultrasonic A-scan was saved in a record consisted of 2048 RF samples per line. The speed of the ultrasound was 1480 m/sec. The data were acquired for phantom within 6 pins at different positions.

Physical Elements Array

In this tool image was reconstructed using physical array elements for linear and phase array probe.

5.2 Main Window:

Figure 5.1: The main window of the tool

The previous window gives the user a background about the new tool which will provide him with a framework for all processing pipeline.

5.3 RF Information Window:

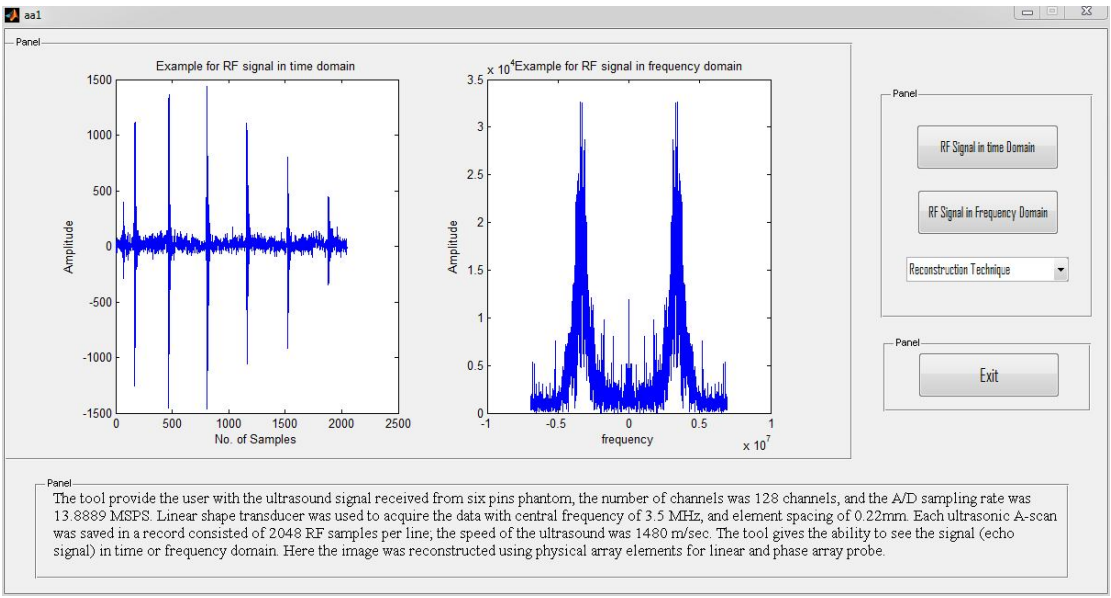

Figure 5.2: The RF signal in time and frequency domain

The above window illustrates the RF signal which is received from six pins phantom in time and frequency domain. The data was acquired using linear shape transducer with central frequency 3.5 MHz.

5.4 Physical Linear array reconstruction

(Images reconstructed using physical array elements for linear array probe)

5.4.1 Primary Reconstruction Windows

Delay Window:

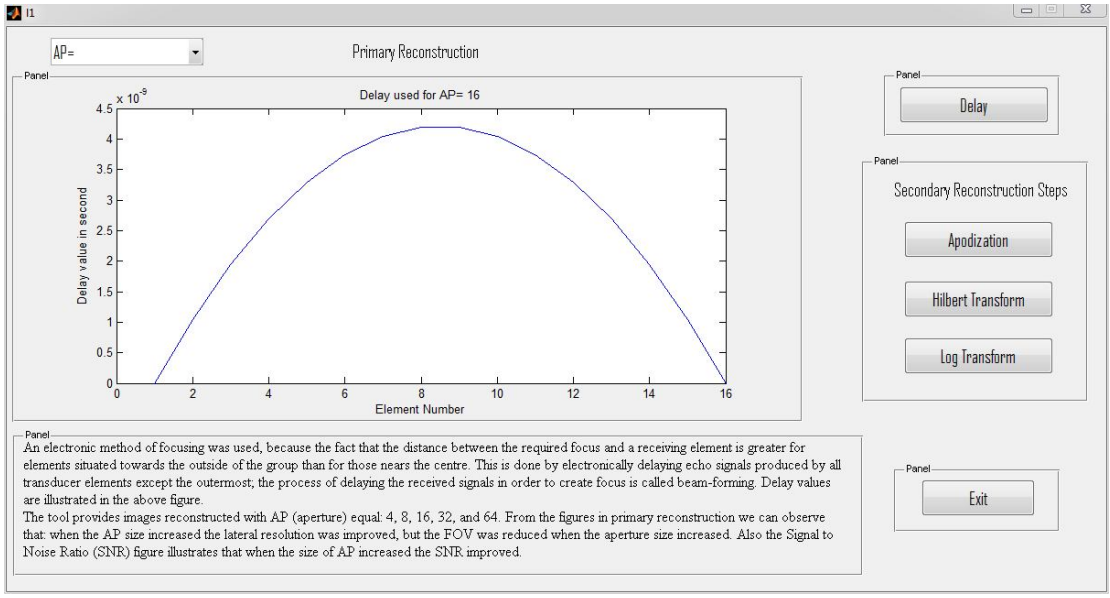

Figure 5.3: The delay used with AP=16

An electronic method of focusing was used, because the fact that the distance between the required focus and a receiving element is greater for elements situated towards the outside of the group than for those nears the centre.

This is done by electronically delaying echo signals produced by all transducer elements except the outermost; the process of delaying the received signals in

order to create focus is called beam-forming. Delay values are illustrated in the previous window.

Six Pin Phantom Images Windows:

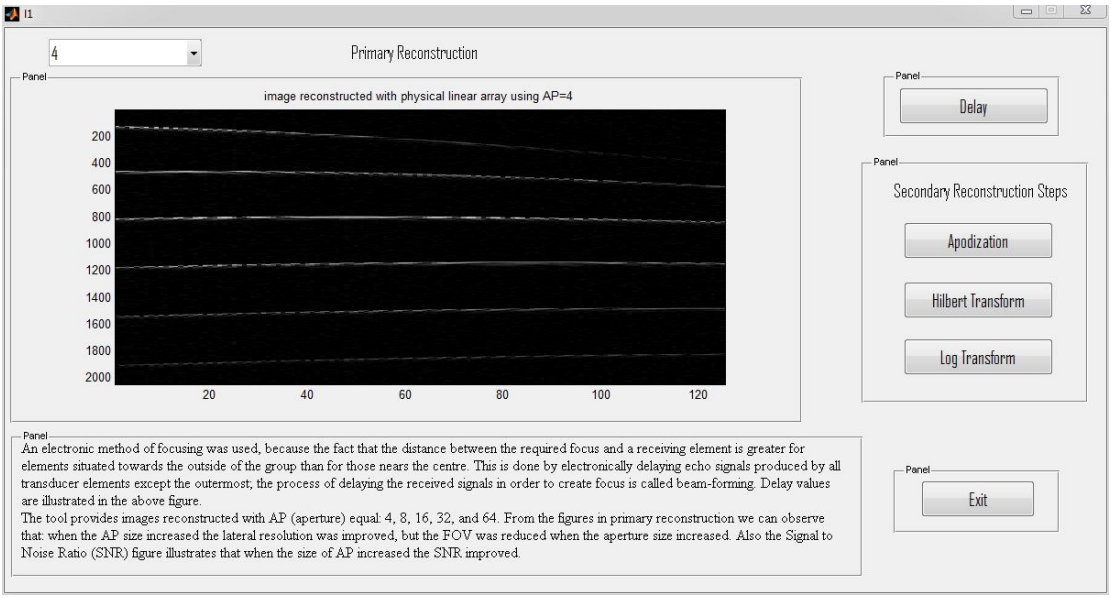

Figure 5.4: Image reconstructed with physical linear array using AP=4

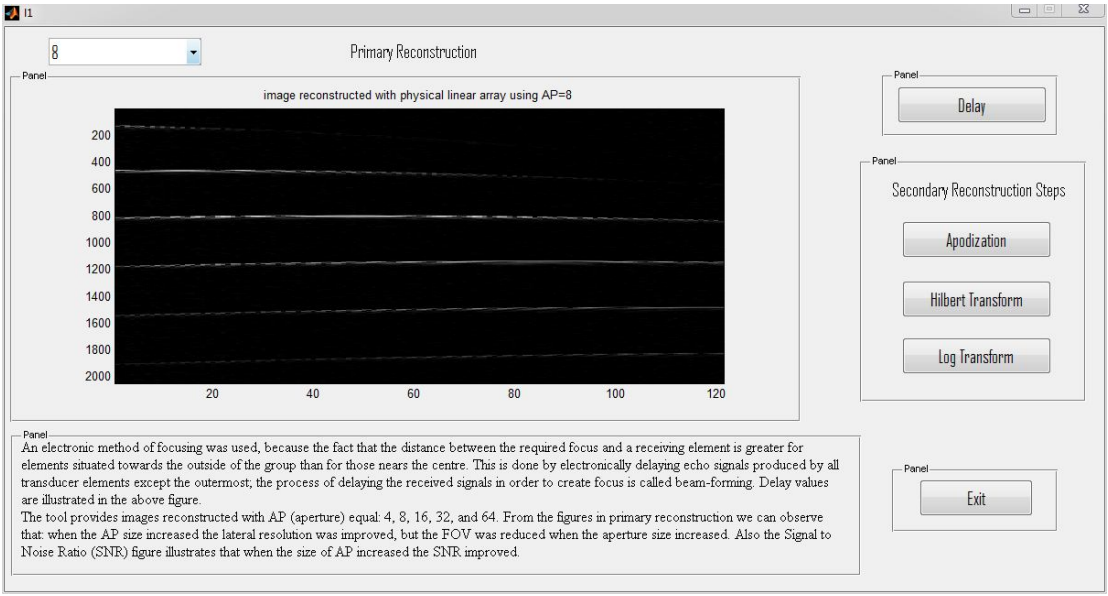

Figure 5.5: Image reconstructed with physical linear array using AP=8

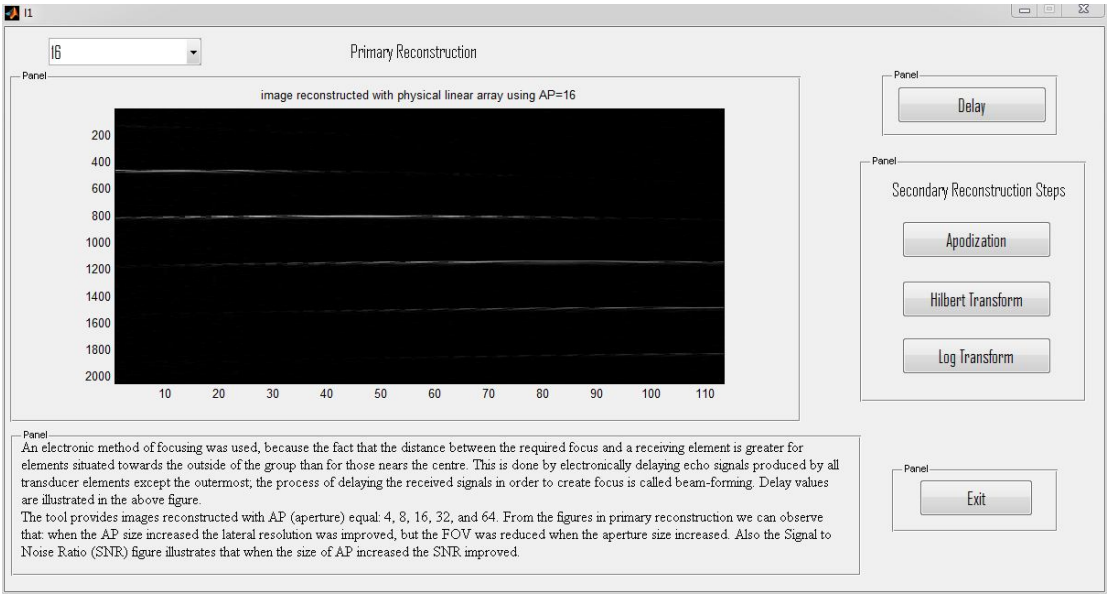

Figure 5.6: Image reconstructed with physical linear array using AP=16

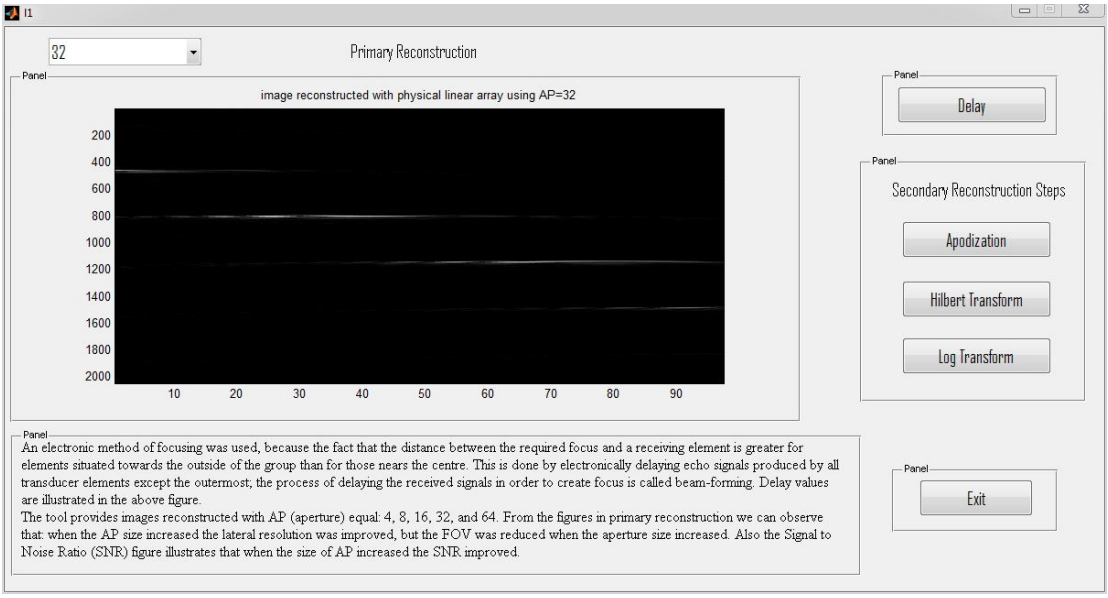

Figure 5.7: Image reconstructed with physical linear array using AP=32

The tool provides images reconstructed using physical linear array with AP (aperture) equal: 4, 8, 16, 32, and 64.

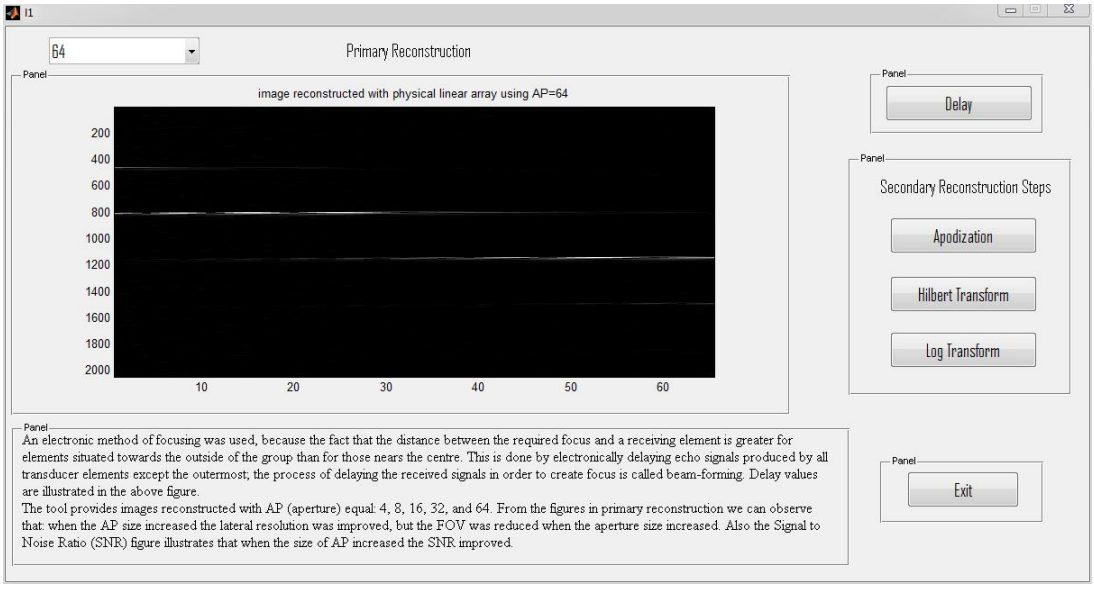

Figure 5.8: Image reconstructed with physical linear array using AP=64

From the above and the next five windows we can observe that: when the AP size increased the lateral resolution was improved, but the FOV was reduced when the aperture size increased.

SNR Window:

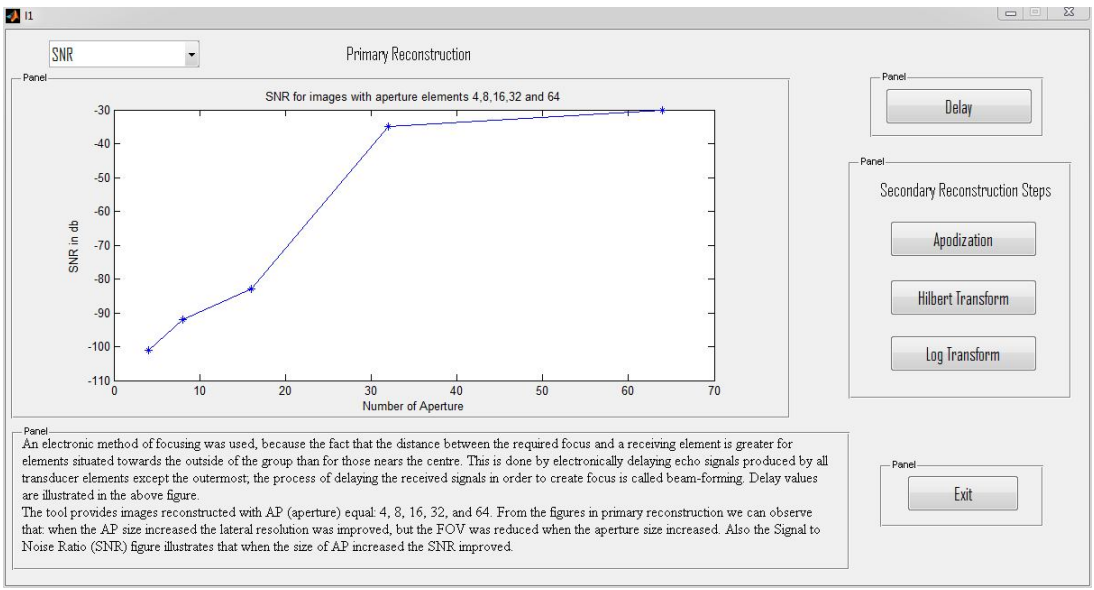

Figure 5.9: SNR for images reconstructed with AP=4, 8, 16, 32 and 64

Besides comparing the previous five images based on lateral resolution and FOV, on the other hand we can use the Signal to Noise Ratio (SNR) to compare the images. The SNR for the five above images was calculated using:

$$SNR = 20\log_{10}\left(\frac{m_a}{s_n}\right)db \qquad \text{(Eq.5-1)}$$

Where, m_a and s_a are average brightness and standard deviation of the images respectively.

The above window illustrates that when the size of AP increased the SNR improved.

5.4.2 Secondary Reconstruction Windows

Apodization Windows:

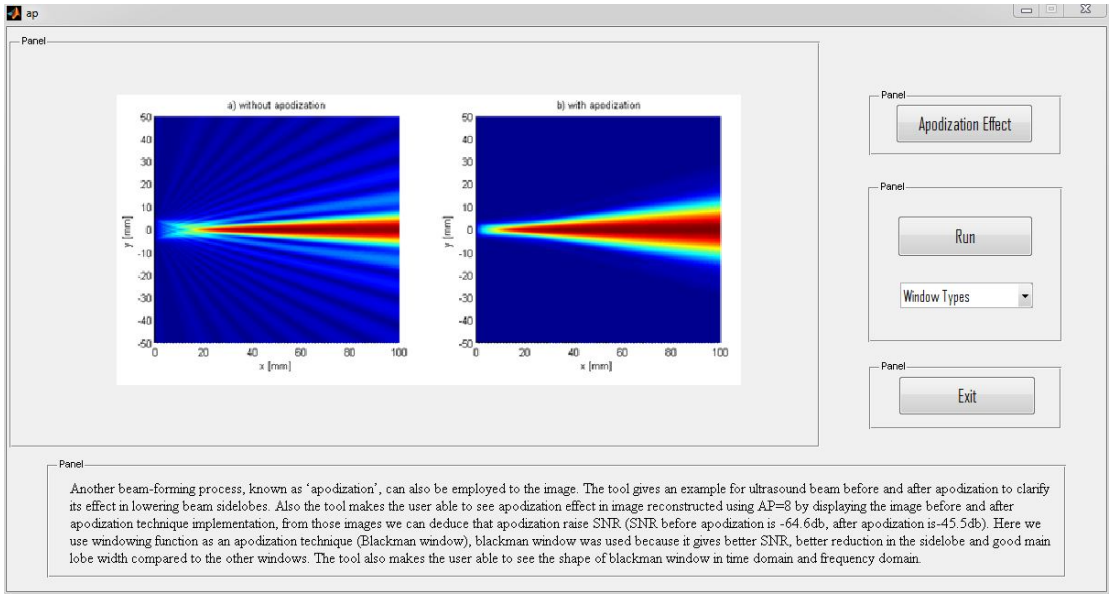

Figure 5.10: Ultrasound beam with and without apodization

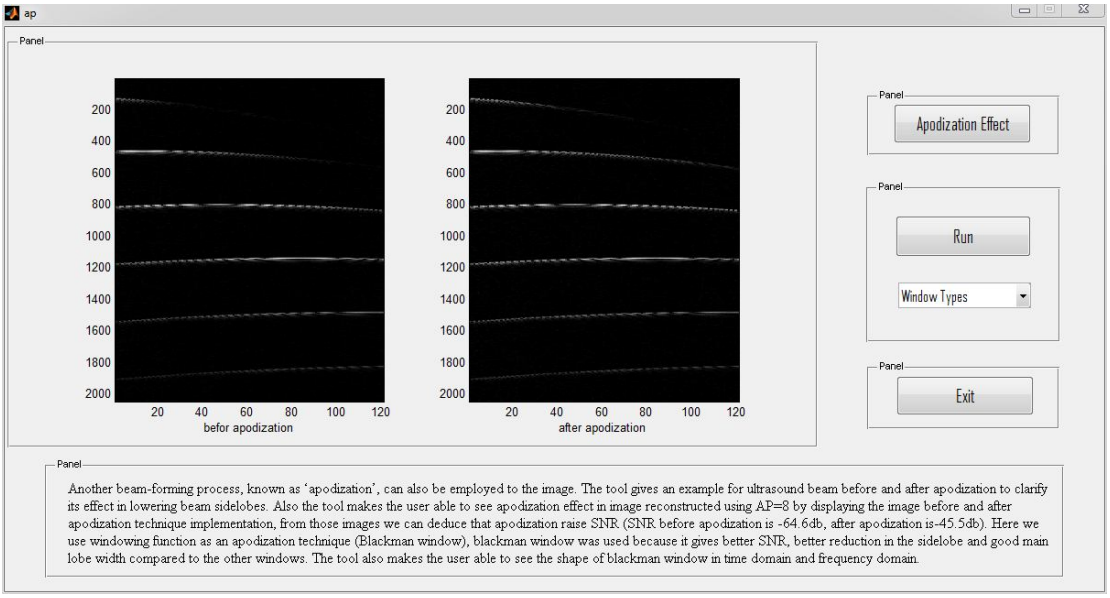

Figure 5.11: Six pins phantom image reconstructed using AP=8 before and after apodization

Another beam-forming process, known as 'apodization', can also be employed to the image. In transmission, this involves exciting the elements non-uniformly, in the reception this can be achieved by giving different amplifications to the signals from each element.

(Figure 5.10) gives an example for ultrasound beam before and after apodization to clarify its effect in lowering beam sidelobes.

Also the tool makes the user able to see apodization effect in image reconstructed using AP=8 by displaying the image before and after apodization technique implementation as shown in (Figure 5.11), from those images we can deduce that apodization raise SNR (SNR before apodization is -64.6db, after apodization is-45.5db).

The next windows show a number of windows in time and frequency domain, it also the show the main-lobes and the side-lobes attenuation for the windows.

The tool makes the user able to see and compare between four types of window: rectangular, hamming, Kaiser (β=4) and blackman. We can compare between the windows from the main-lobe width and the side-lobe attenuation point of view.

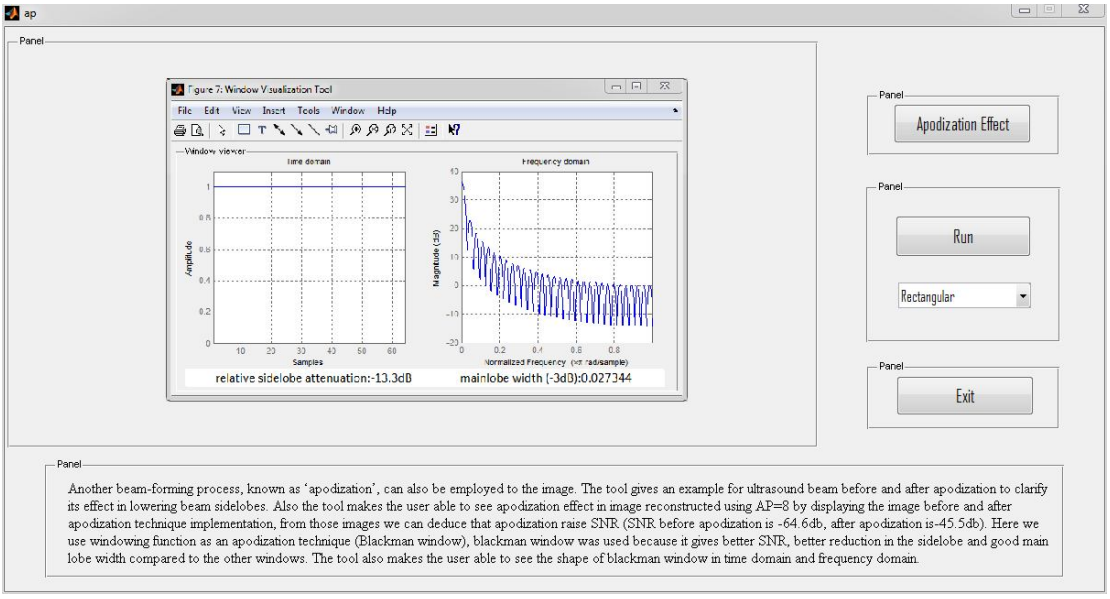

Figure 5.12: Rectangular window of length 16 in time and frequency domain

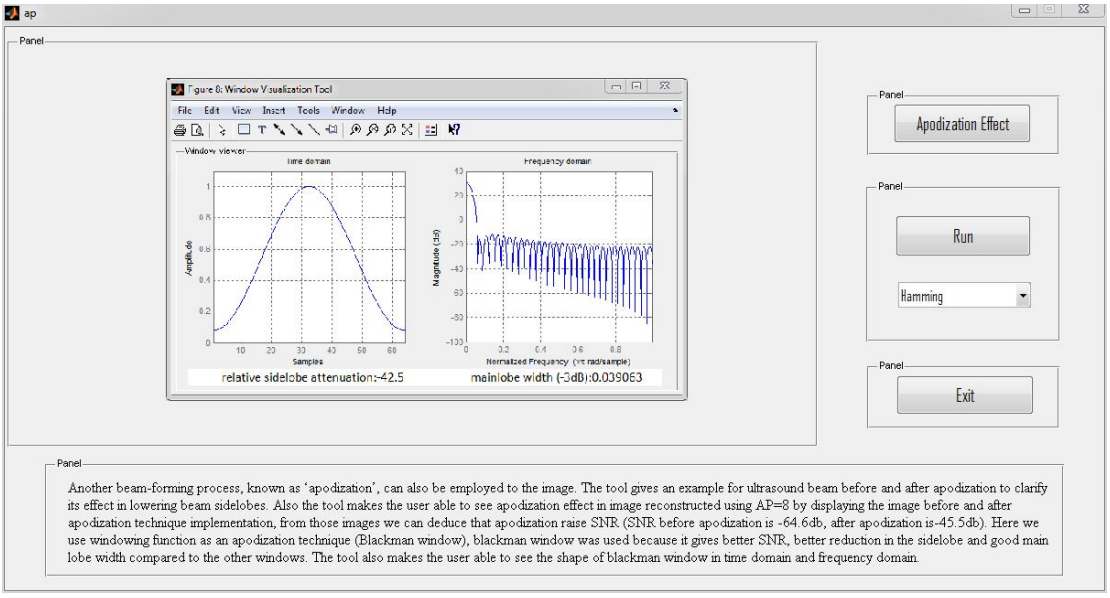

Figure 5.13: Hamming window of length 16 in time and frequency domain

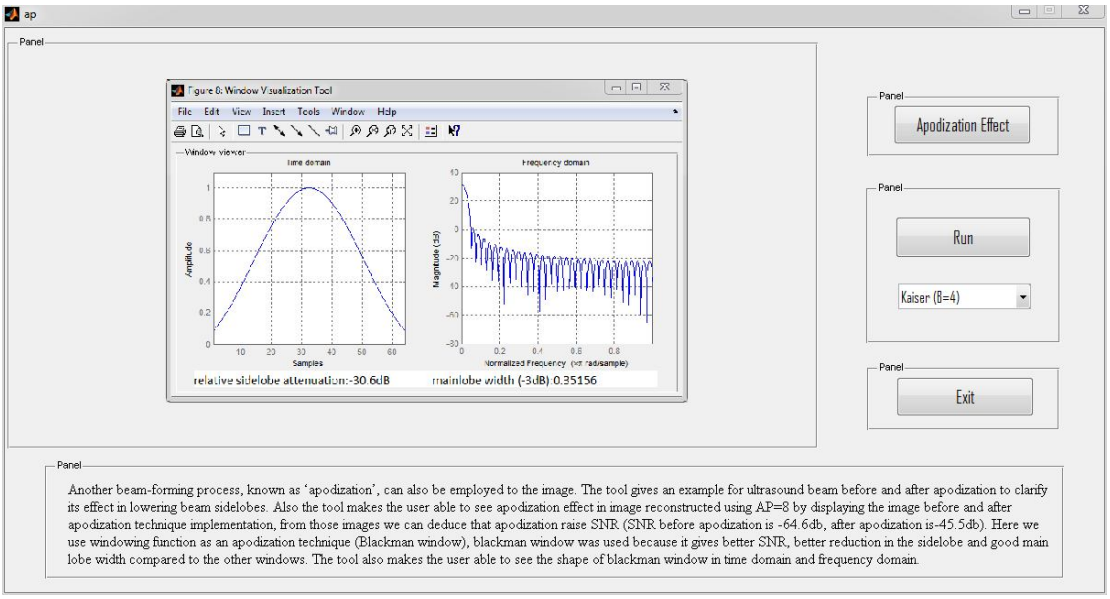

Figure 5.14: Kaiser (β=4) window of length 16 in time and frequency domain

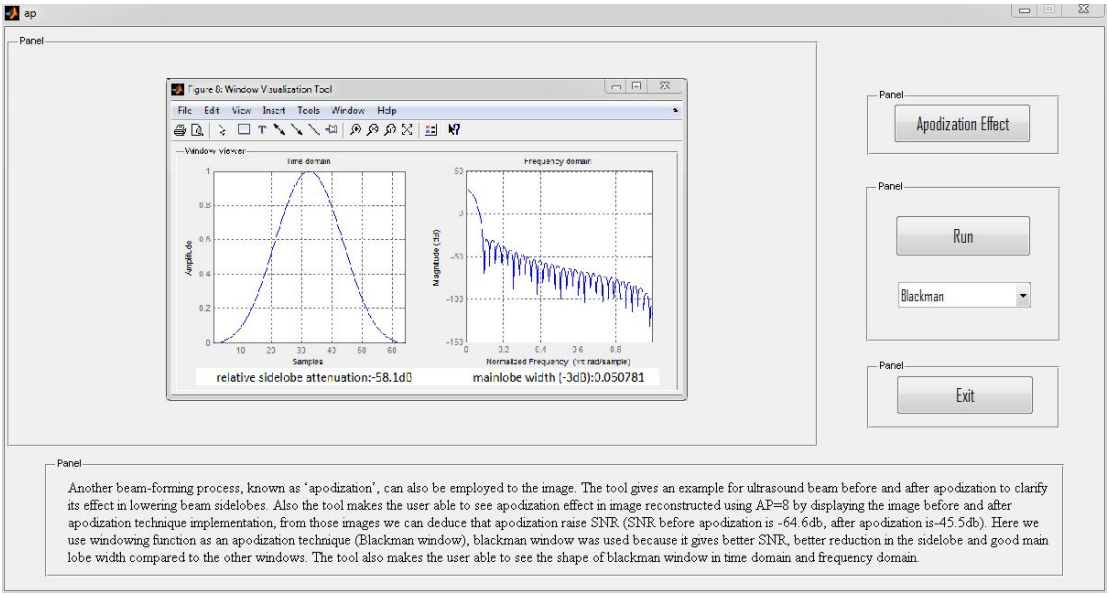

Figure 5.15: Blackman window of length 16 in time and frequency domain

In this tool windowing function was used as an apodization technique (Blackman window), blackman window was used because it gives better SNR, better reduction in the side-lobe and good main lobe width compared to the

other windows [2]. The tool also makes the user able to see the shape of blackman window in time domain and frequency domain (Figure 5.15).

Hilbert Transform Windows:

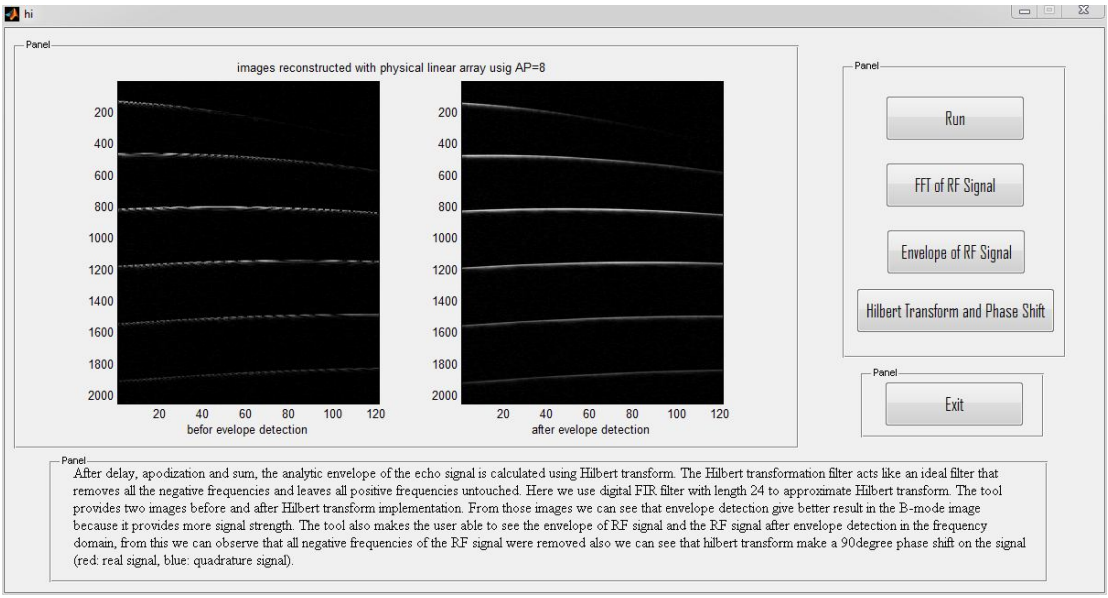

Figure 5.16: Image reconstructed using AP=8 before and after envelope detection

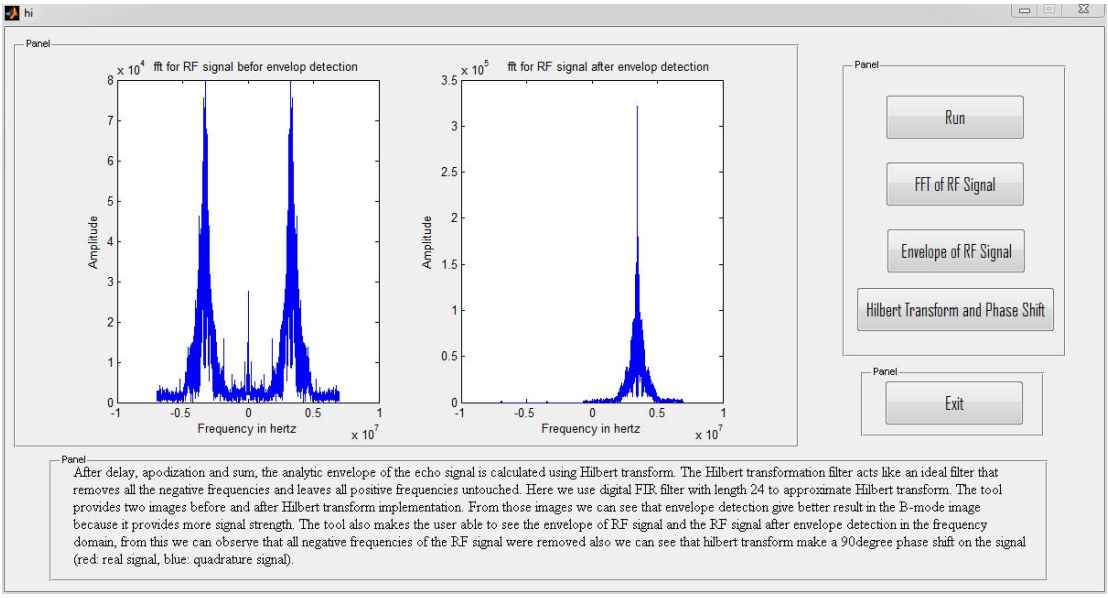

Figure 5.17: RF signal before and after envelope detection in the frequency domain

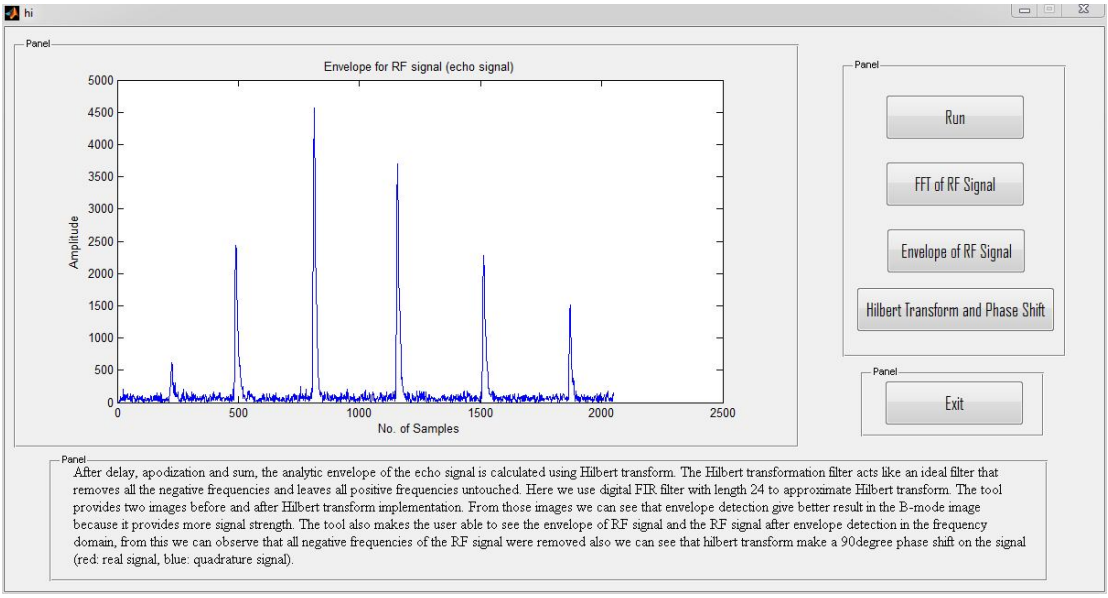

Figure 5.18: The envelope of RF signal in time domain

After delay, apodization and sum, the analytic envelope of the echo signal is calculated using Hilbert transform. The Hilbert transformation filter acts like an ideal filter that removes all the negative frequencies and leaves all positive frequencies untouched. Here we use digital FIR filter with length 24 to approximate Hilbert transform.

The tool provides two images before and after Hilbert transforms implementation as shown in (Figure 5.16). From those images we can see that envelope detection give better result in the B-mode image because it provides more signal strength.

The tool also makes the user able to see the envelope of RF signal in time domain as in (Figure 5.18), from this figure we can ensure that envelope is a non negative curve that connects the peaks (negative peaks are inverted) of the signal.

The tool also display the RF signal after envelope detection in the frequency domain as in (Figure 5.17), from this we can observe that all negative frequencies of the RF signal were removed.

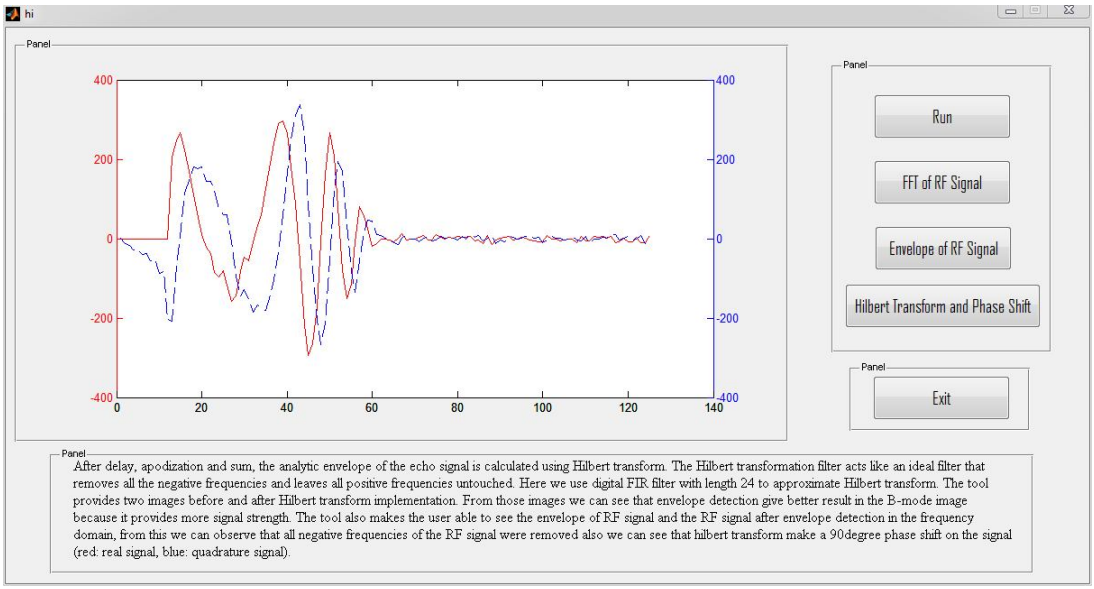

Figure 5.19: The analytical envelope (real and quadrature signal)

Log Transform Windows:

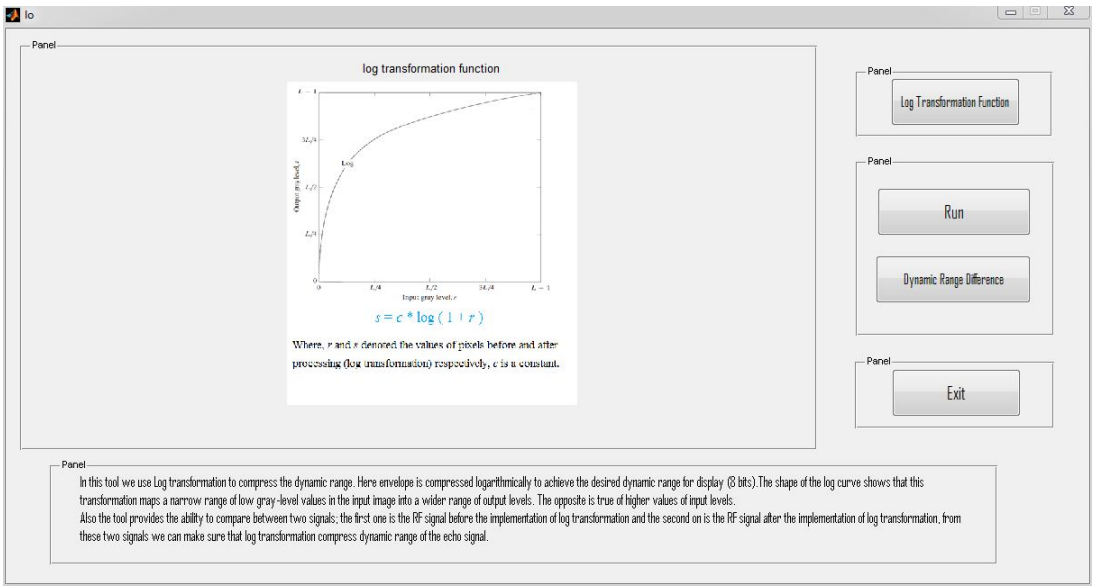

Figure 5.20: Log transformation function

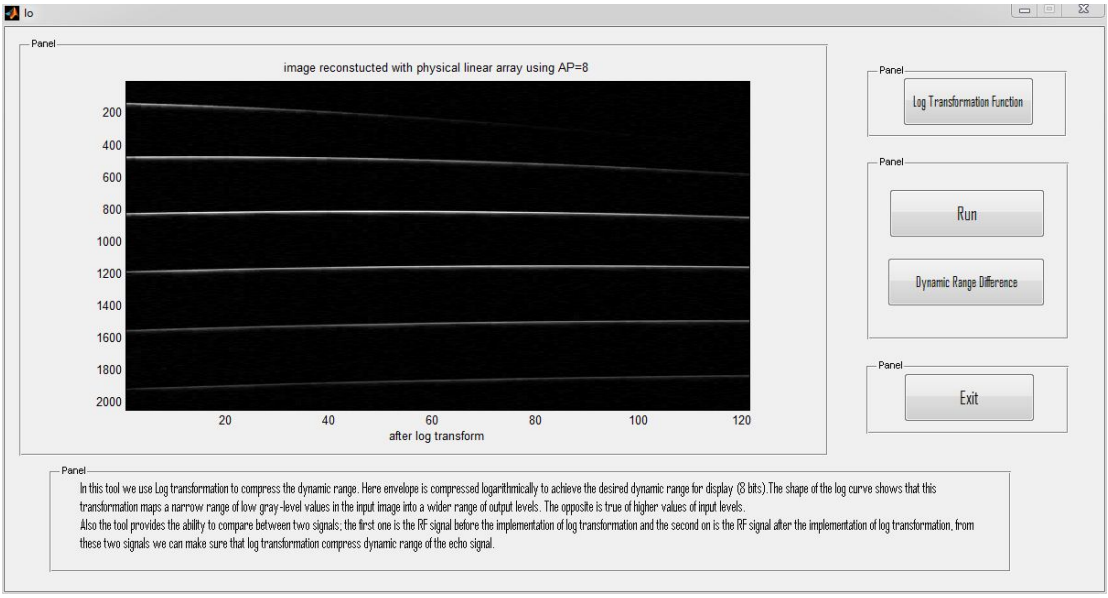

Figure 5.21: Image reconstructed using AP=8 after log transformation

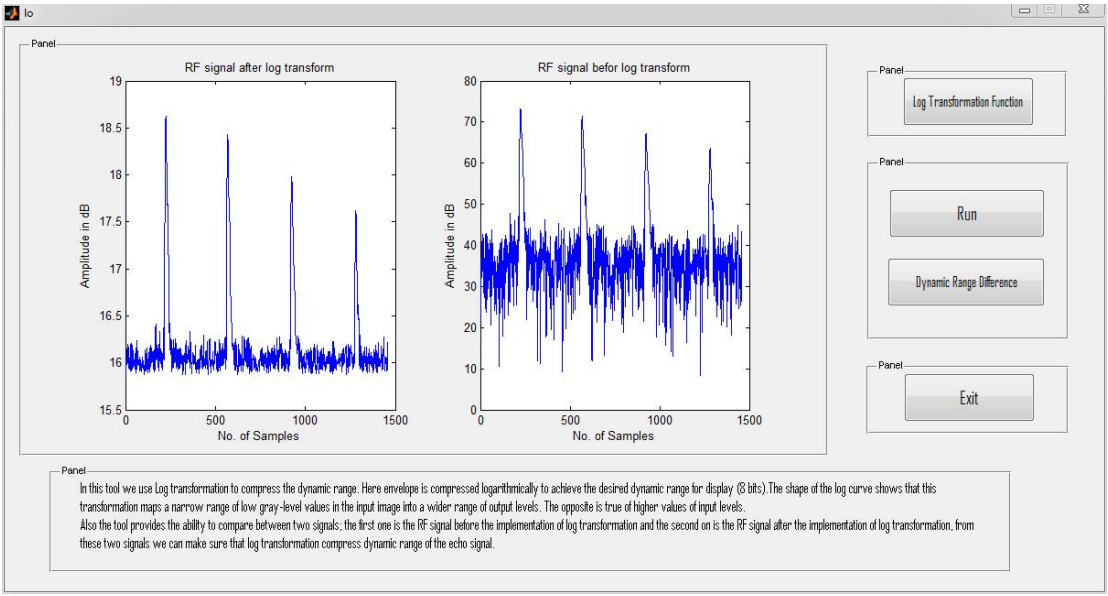

Figure 5.22: RF signal in time domain before and after log transformation

In this tool we use Log transformation to compress the dynamic range. Here envelope is compressed logarithmically to achieve the desired dynamic range for display (8 bits).

The shape of the log curve shows that this transformation maps a narrow range of low gray-level values in the input image into a wider range of output levels. The opposite is true of higher values of input levels as in (Figure 5.20). (Figure 5.21) show image reconstructed using AP=8 after applying log transformation. Also the tool provides the ability to compare between two signals; the first one is the RF signal before the implementation of log transformation and the second on is the RF signal after the implementation of log transformation as in (Figure 5.22), from these two signals we can make sure that log transformation compress dynamic range of the echo signal.

5.5 Physical Linear phase array reconstruction

(Images reconstructed using physical array elements for phase array probe)

In this situation image was reconstructed using raster point technique, element number 128 was the transmitter and received with all 128 elements. Also over sampling technique was used to achieve high resolution. However, this will increase the data volume has to acquire. This is usually avoided by sampling just above the Nyquist rate and interpolating to achieve the required resolution. As shown in table B in the appendix; when sampling ratio (F) increased the resolution decreased. From the table the resolution equal to (1/ (2×sampling ratio)).

5.5.1 Primary Reconstruction Window

Due to the small FOV of the linear reconstruction and its limited lateral resolution linear phase reconstruction technique was used to reconstruct image of six pins phantom from the data set.

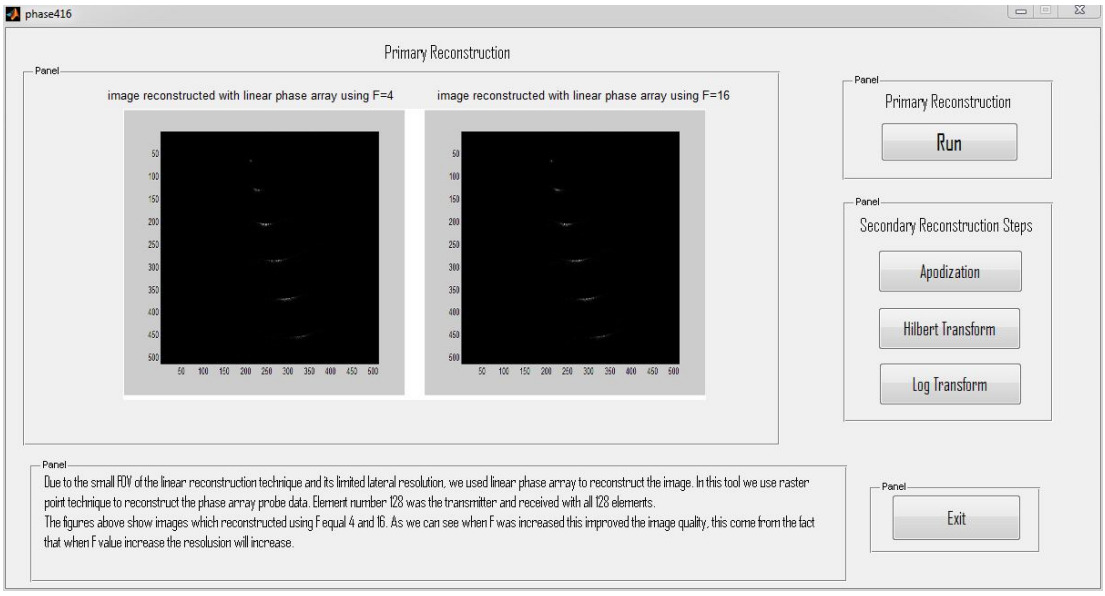

Figure 5.23: Images reconstructed with physical phase linear array using F=4, 16

As shown in (Figure 5.23) image was reconstructed using F equal 4 and 16. From the above figure we can observe that increment of F improve the image quality.

5.5.2 Secondary Reconstruction Windows

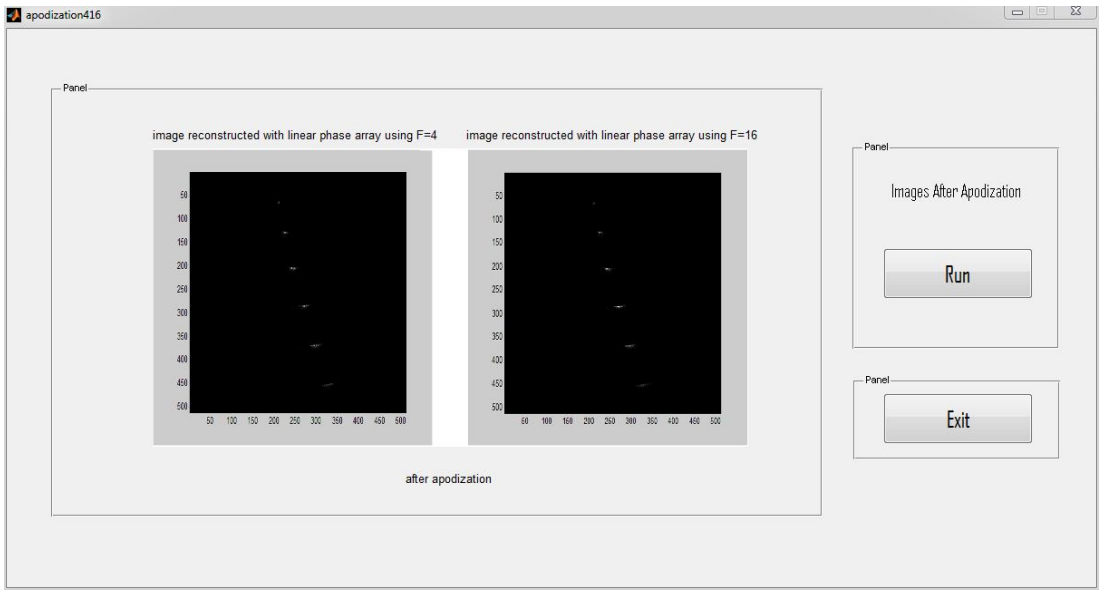

Figure 5.24: Images reconstructed using F=4, 16 after apodization

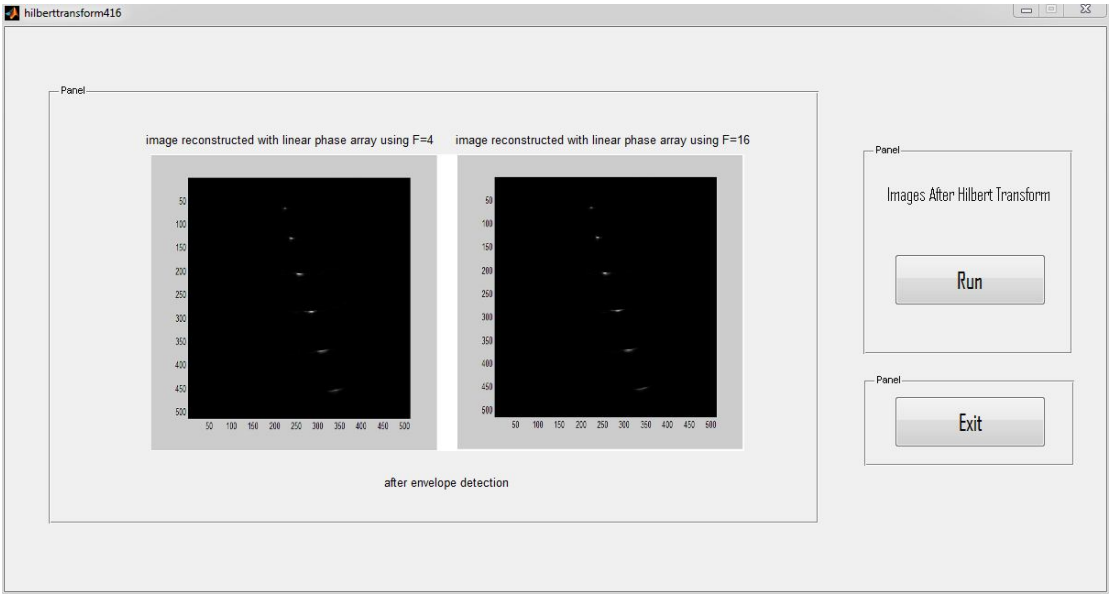

Figure 5.25: Images reconstructed using F=4, 16 after envelope detection

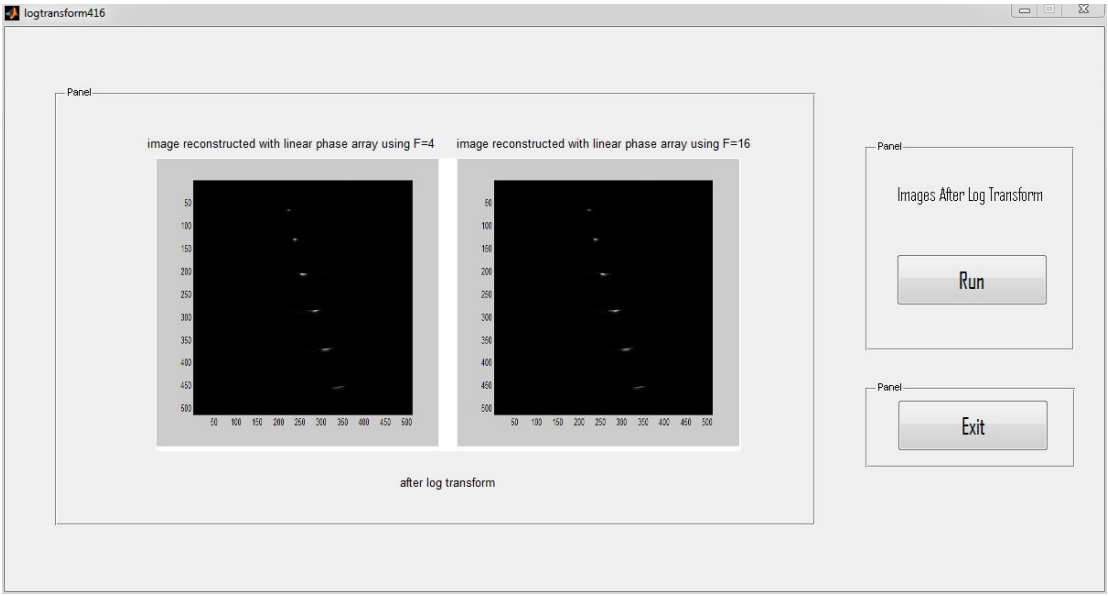

Figure 5.26: Images reconstructed using F=4, 16 after log transform

The above three windows show the secondary reconstruction techniques:

Apodization Technique:

Which used to lower the beam side-lobes, windowing function was used as apodization technique. Here we choose blackman window according to the information in the appendix (table A).

Hilbert Transform:

This used to calculate the analytic envelope of RF signal. FIR Hilbert transform filter with length 24 was used to obtain the quadrature components of RF signal. As can be viewed from (Figure 5.25) the results were better than (Figure 5.23), because the envelope provided more signal strength.

Log Transformation:

This used to compress the envelope signal logarithmically in order to achieve the desired dynamic range for display (8 bits).

CHAPTER Six

6. Conclusion AND Future Works

6.1 Conclusion

In this study we apply signal processing methodologies for digital beam-forming, delays were calculated using equations in chapter three, black-man window was used as apodization technique because it has good attenuation for side-lobes. We reconstruct image using: linear array reconstruction technique with aperture equal 4, 8, 16, 32, 64 and linear phase array reconstruction technique with sampling frequency 4 and 16. FIR Hilbert transform with length 24 was used to obtain quadrature component of analytical signal after that envelope detection was calculated. Finally dynamic range compression was applied on the signal using Log transform to achieve the desired dynamic range for display (8 bits). Also In this thesis we used correct data obtained from the Biomedical Ultrasound Laboratory, University of Michigan; the phantom data set that was used to generate the results here is under "Acusonl7".

6.2 Future Works

The tool can be developed by adding:

1- The ability to choose window type like rectangular, hamming and Kaiser for apodization and compare the results.

2- The virtual array elements reconstruction technique beside the physical array elements technique to reconstruct ultrasound image.
3- Helps icon to give the students more information about the process of converting RF ultrasound data into B-mode image.
4- Database which contains a number of ultrasound data sets.

REFERENCES

[1] Guy. C and Ffytche, D, (2005), An Introduction to the Principles of Medical Imaging:Inc NetLibrary - Imperial College Press, Distributed by World Scientific Pub, 374-385.

[2] Hassan Mawia. A and Kadah. Y. M, (2013), 'Digital Signal Processing Methodologies for Conventional Digital Medical Ultrasound Imaging System', American Journal of Biomedical Engineering, 3(1), 14-30.

[3] Bronzino. J, (2004), Diagnostic Ultrasound Imaging: Inside Out, Series Editor Trinity College - Hartford, Connecticut, 22-36.

[4] Edler. I, Lindstrom. K, (2004), 'The history of echocardiography', Ultrasound Med Biol, 30, 1565-1644.

[5] Abd-Elmoniem. K. Z, Youssef. A. M and Kadah. Y. M, (September 2002), 'Real-Time Speckle Reduction and Coherence Enhancement in Ultrasound Imaging via Nonlinear Anisotropic Diffusion', IEEE Transactions Biomedical Engineering, 49(9), 997-1014.

[6] Kreindler. D, (Septemper 2010), 'The Future of Beam-forming in Ultrasound', Samplify Systems, Santa Clara.

[7] Pesque1. P and Souquet. J, (September 1999), 'Digital ultrasound: from beam-forming to PACS', IEEE Transactions on Ultrasonics, 43(3), 11-26.

[8] Zagzebski. J. A, (1996), 'Essentials of ultrasound physics', St Louis, Mo: Mosby.

[9] Reeder. R and Petersen. C, (2007), 'The AD9271-A Revolutionary Solution for Portable Ultrasound', Analog Dialogue, Analog Devices.

[10] Hassan. Mawia. A, (January-2015), 'Compact Low-Cost Digital Medical Ultrasound Imaging System', International Journal of Scientific & Engineering Research, 6(1), 210-216.

[11] Hendee. W. R and Russell. R. E, (2002), Medical Imaging Physics, Fourth edition, New York: John Wiley & Sons, 303-353.

[12] Hoskins. P, Martin. K. A, (2010), Diagnostic Ultrasound Physics and Equipment, Second Edition, Cambridge University Press, 14-57.

[13] Kino. G. S, (1987), ‘Acoustic wave’s devices imaging and analog signal processing’, Englewood Cliffs: Prentice Hall.

[14] Aldrich. J. E, (2007), ‘Basic physics of ultrasound imaging’, Society of Critical Care Medicine and Lippincott Williams & Wilkins, 35(5), 131–137.

[15] Otto. C. M, (2000), ‘Principles of echocardiographic image acquisition and Doppler analysis’, Textbook of Clinical Ecocardiography, 2nd edition, Philadelphia, 1–29.

[16] Lawrence. J. P, (2007), ‘Physics and instrumentation of ultrasound’, Crit Care Med, 35, 314–322.

[17] Hendee. W. R, Holmes. J. H, Fullerton. G. D and Zagzebski. J. A, (1980), ‘History of Ultrasound Imaging’, New York: American Institute of Physics.

[18] Chan. W. S, (2009), ‘Ultrasound Imaging for Regional Anesthesia’, 2nd edition, Toronto, ON: Toronto Printing Company, 24, 134-142.

[19] Dickinson. R. J, (1986), ‘Reflection and scattering of ultrasound’, Physical Principles of Medical Ultrasonics, Chichester: Ellis Horwood.

[20] Duck. F. A, (2002), ‘Nonlinear acoustics in diagnostic ultrasound’, Ultrasound in Medicine and Biology, 28, 1-18.

[21] Middleton. W, Kurtz. A and Hertzberg. B, (2004), Practical physics in ultrasound, the Requisites. 2nd edition, St Louis, MO: Mosby, 3-27.

[22] Suslick. K. S, (1988), ‘Ultrasound: It’s Chemical, Physical and Biological Effects’, New York, VCH Publishers, 20, 81–102.

[23] Roberts. P. A and Williams. J, (2008), Farr's Physics for Medical Imaging, Second edition, Philadelphia: Saunders Elsevier, 147-168.

[24] Tranquart. F, Grenier. N, Eder. V and Pourcelot. L, (1999), ‘Clinical use of ultrasound tissue harmonic imaging’, Ultrasound in Medicine and Biology, 25, 89 -94.

[25] Kaur. K, (March 2013), ‘Digital Image Processing in Ultrasound Images’, International Journal on Recent and Innovation Trends in Computing and Communication, 1(4), 388 -393.

[26]http://www.livestrong.com/article/250785-how-does-ultrasound equipment work/ Ultrasound Equipments, January 2013.

[27] Chiao. R. Y and Hao. X, (2003), 'Coded excitation for diagnostic ultrasound: A system developer's perspective', IEEE Ultrason Symp Proc, 437-448.

[28] Cole. C. R, (1991), 'Properties of swept FM waveforms in medical ultrasound imaging', IEEE Ultrason Symp Proc, 1243-1248.

[29] Entrekin. R. R, Jago. J. R and Kofoed. S. C, (2000), 'Real-time spatial compound imaging: Technical performance in vascular applications', Acoustical Imaging, Kluwer Academic/Plenum Publishers, New York, 25, 331-342.

[30] Prince. J. L and Links. J. M, (2013), 'Ultrasound Imaging', Ultrasound Imaging Modes, NY 11201, 27-37.

[31] Kasai. C, Namekawa. K, Koyano. A and Omoto. R, (May 1985), 'Real-Time Two-Dimensional Blood Flow Imaging Using an Autocorrelation Technique', IEEE Transactions on Sonics and Ultrasonic, 32(3), 458-464.

[٣٢] Levi. S, (1997), 'The history of ultrasound in gynecology 1950-1980', Ultrasound in Medicine & Biology, 23(4), 481-552.

[33] Donald. I, (1998), 'Sonar- A new diagnostic echo-sounding technique in obstetrics and gynecology', Proceedings of the Royal Society of Medicine, 55(8), 637-645.

[34] Guy. C and fftyche. D, (2000), 'An Introduction to the Principles of Medical Imaging', Imperial College Press, London.

[35] Hussey. M, (1985), 'Basic Physics and Technology of Medical Diagnostic Ultrasound', MacMillan and Sons, London.

[36] McDicken. W, (1976), 'Diagnostic Ultrasonics', New York, John Wiley & Sons, 248-300.

[37] Bumber. J. C and Tristam. M, (1988), 'Diagnostic ultrasound: Physics of Medical Imaging', Philadelphia, Adam Hilger, 319-388.

[38] Lisciandro. G. R., (2014), Focused Ultrasound Techniques for the Small Animal Practitioner, First Edition, Published by John Wiley & Sons.

[39] Thomenius. K. E, (1996), 'Evolution of Ultrasound Beam-formers', IEEE Ultrasonics Symposium, 1615-1622.

[40] Sorner. J. C, (1968), ‘Electronic sector scanning for ultrasonic diagnosis’, IEEE Ultrasonics Symposium, 6, 153-159.

[41] Vonramm. O. T and Thurstone. E. L, (1970), ‘Thaurnascan: Improved image quality and clinical usefulness’, Ultrasound in Medicine, Plenum Press, NY, 2, 463-496.

[42] Thurstone. F. L, Vonramm. O. T, (1974), ‘A New Ultrasound Imaging Technique Employing Two-Dimensional Electronic Beam Steering’, Ultrasound in Medicine, American Elsevier Publishing Co., New York, 43-48.

[43] Kisslo. J. A, Vonramm. O. T and Thurstone. F. L, (1977), Clinical Results of Real-Time Ultrasonic Scanning of the Heart Using a Phased Array System, Ultrasound in Medicine, 3th edition, 1547-1558.

[44] Tancrell. R. H, Callerame. J and Wilson. D . T, (1978), ‘Near-field, transient acoustic beam-forming with arrays’, Ultrasonics Symposium Proceedings, IEEE 78CH1344- ISU, 339-343.

[45] Eaton. M. D, Melen. R. D and Meindl. D, (1980), ‘A flexible, real- time system for experimentation in phased-array ultrasound imaging’, Acoustic Imaging, 8, edited by Metherell. A. F, Plenum Press, New York, 55-67.

[46] Karrer. H. E, Dias. J. F, Larsun. I. D and Pering. R. D, (1980), ‘A phased array acoustic imaging system for medical use’, Ultrasonics Symposium Proceedings, IEEE ROCH1602- 2, 757-762.

[47] Wright. J, (1985), ‘Resolution issues in medical ultrasound’, IEEE Ultrasonics Symposium Prnceedings, IEEE XSCH 2209-5, 793-799.

[48] Walker. J. T and Meindl. J. D, (1975), ‘A digitally controlled CCD dynamically focused phased array’, Ultrasonics Symposium, 80-83.

[49] Burckhardt. C. B, Grandchamp. P. A, Hoffman. H and Fehr. R, (1979), ‘A simplified ultrasound phased arrays sector scanner’, Echo-cardiology, 385-393.

[50] Manes. G. F, Atzeni. C and Susini. C, (1983), ‘Design of **a** simplified delay system for ultrasound phased array imaging’, IEEE Transactions of Sonica Ultrasonics, 30, 350-354.

[51] Thurstone. F. L and Vonramm. O. T, (1973), ‘A new ultrasound imaging technique employing two-dimensional electronic beam steering’, Acoustical holography, 16(15), 249–259.

[52] Vonramm. O. T and Thurstone. F. L, (1976), 'Cardiac imaging using a phased-array ultrasound system', System-design Circulation, 53(2), 258-262.

[53] Talman. J, Garverick. S and Lockwood. G, (2003), 'Integrated circuit for high-frequency ultrasound annular array', Proceedings of the IEEE Custom Integrated Circuits Conference, 477-480.

[54] King. D. L, (1974), 'Real-time cross-sectional ultrasonic imaging of the heart using a linear array multi-element transducer', J. Clin. Ultrasound, 2, 222-240.

[55] Vasudevan. S, (September 1998), 'Ultrasonic Digital Beam-formation: A Comparative Study', IEEE Transactions on Ultrasonics, 400-425.

[56] Gray. P. R and Meyer. R. G, (1993), 'Analysis and design of analog integrated circuits', Hamilton Printing.

[57] Pridham. R. G and Mucci. R. A, (1979), 'digital interpolation beam-forming for low-pass and band-pass signal', proc.IEEE, 67(6), 904-919.

[58] Ozaki. Y**,** Sumitani. H, Tomoda. T and Tanaka. M, (November 1988), 'A New System for Real-Time Synthetic Aperture Ultrasonic Imaging', IEEE Transactions on Ultrasonic's, Ferroelectrics and Frequency Control, 35(6).

[59] Hazier. C. H and O'Brien. W. D, (1996), 'Synthetic Aperture Imaging with a Virtual Source Element', Bioacoustics Research Laboratory, Department of Electrical and Computer Engineering, University of Illinois, IEEE Ultrasonics Symposium.

[60] Passman. C and Ermert. H, (July 1996), 'A 100 MHz ultrasound imaging system for dermatologic and ophthalmologic diagnostics', IEEE Transaction Ultrasonic's, Ferro-electrics, frequency Control, 43(4), 545-552.

[61] Chiao. R. Y, Thomas. L. J and Silverstein. S. D, (1997), 'Sparse Array Imaging With SPATIALLY-Encoded Transmits', GE Corporate Research and Development, IEEE Ultrasonic's Symposium.

[62] Cooley. C. R and Robinson. B. S, (1994), 'Synthetic Focus Imaging Using Partial Datasets', IEEE Ultrasonic's Symposium, 1539-1542.

[63] Lockwood. G. R and Foster. F. S, (1995), 'Design of Sparse Array Imaging Systems', IEEE Ultrasonic's Symposium, 1237-1243.

[64] Walker. W. F and Trahey. G. E, (1994), 'Real-Time Synthetic Receive Aperture Imaging: Experimental Results', IEEE Ultrasonic's Symposium, 1657-1660.

[65] Hassan. Mawia. A, Youssef. A. M and Kadah. Y. M, (2011), 'Modular FPGA-Based Digital Ultrasound Beam-forming', Systems & Biomedical Engineering Department, Cairo University, IEEE.

[66] Jensen. J. A, (2000), 'Ultrasound imaging and its Modeling', Department of Information Technology, Technical University of Denmark, Denmark.

[67] Christensen. D. A, (1988), 'Ultrasonic Bioinstrumentation', Jonh Wiley & Sons, New York.

[68] Shin. H. J, Kwan. J. R and Song. S. J, (September 2001), 'Ultrasonic Real Time Imaging Technique for the Inspection of Electro-fusion Joints for Polyethylene Piping', Forum for Gas Safety, edited by Korea Gas Safety Corporation, 21-37.

[69] Oppenheim. A. V and Schafer. R. W, (1989), 'Discrete-Time Signal Processing', NJ: Prentice-Hall, Englewood Cliffs.

[70] Troncoso. D. E and Dolecek. G. J, (2012), 'Digital FIR Hilbert Transformers: Fundamentals and Efficient Design Methods', INTECH, 1, 445-482.

[71] Gonzalez. R. C, (2001), Digital Image Processing, Second Edition, University of Tennessee, Publisher, Tom Robbins, 85-90.

[72] www.Mathworks.com/ MATLAB 7.10.0 (R2010a)/ Creating Graphical User Interface.

[73] Silver. H, (2013), 'Creating Graphical User Interfaces with MATLAB', Fairleigh Dickinson University, Mid-Atlantic Section Conference of the American Society of Engineering Education, 189-221.